2025-06-26

Directivity and Sound Radiation of Percussion Instruments and Harmonic Analysis of the Alto Saxophone

Hanna Michelle Pavill
Brigham Young University

Directivity and Sound Radiation of Percussion Instruments and Harmonic Analysis of the Alto Saxophone

Hanna Michelle Pavill

A thesis submitted to the faculty of
Brigham Young University
in partial fulfillment of the requirements for the degree of

Master of Science

Micah R. Shepherd, Chair
Brian E. Anderson
Richard L. Sandberg

Department of Physics and Astronomy

Brigham Young University

ABSTRACT

Directivity and Sound Radiation of Percussion Instruments and
Harmonic Analysis of the Alto Saxophone

Hanna Michelle Pavill
Department of Physics and Astronomy, BYU
Master of Science

This thesis investigates how musical instruments radiate sound, with a focus on directional behavior under realistic performance conditions. High-resolution measurements using a rotating microphone array were used to study percussion and woodwind instruments, providing new insight into how design, excitation, and frequency content shape acoustic output.

The first set of experiments analyzed the directivity of the bass drum, triangle, and open snare. Each instrument exhibited unique radiation patterns reflecting its structure and playing method. The bass drum showed dipole-like behavior at low frequencies, transitioning to omnidirectional spreading at mid frequencies, and increasingly irregular patterns at higher frequencies. The triangle, due to its rigid and open-frame design, produced sharp directional lobes, especially at high frequencies. The open snare demonstrated complex frequency-dependent behavior influenced by interactions between its shell, heads, and cavity. Together, these results highlight how percussion instrument radiation depends on both structural geometry and striking technique.

The next experiment focused on the glockenspiel, comparing the radiated sound from a fully mounted instrument to that of an individual bar under different boundary conditions. At low frequencies, the full instrument's behavior matched that of a bar mounted on a rigid baffle, suggesting strong influence from the supporting frame. At higher frequencies, the directivity more closely resembled that of an unbaffled bar, indicating that bar-specific modal behavior becomes dominant. Scanning laser Doppler vibrometry confirmed these observations by visualizing both bending and torsional modes of vibration.

The final investigation explored the alto saxophone by analyzing the radiated sound from the same B flat pitch played in three registers. The results showed that while the low B flat radiated primarily from the bell, the middle and high B flats exhibited similar patterns resembling distributed sources along the instrument's body, consistent with a phased line array. Spectral analysis revealed stable harmonic spacing but register-dependent changes in energy distribution and directionality.

Overall, this work provides new high-resolution data on instrument directivity and demonstrates how structural features, mounting, and register impact radiated sound. These findings offer practical value for acoustic modeling, microphone placement, and the design of musical performance and recording spaces.

Keywords: Musical acoustics, Directivity, Percussion instruments, Wind instruments, Sound Radiation

ACKNOWLEDGMENTS

I would first like to express my gratitude to my advisor, Dr. Micah Shepherd, for his guidance, encouragement, and support throughout this project. His insights and feedback were instrumental in shaping the direction of this research and helping me grow as both a student and a researcher.

I would also like to thank Dallin Harwood, Micah Hattaway, Jacob Hales, and Emma Todd for their help with measurements. Additionally, I am grateful to Jacob Sampson and Jeremy Peterson for their work in constructing equipment used in the measurement process.

I would also like to thank my family for their unwavering support and encouragement. During late nights and long stretches of writing and analysis, their patience, understanding, and belief in me kept me motivated.

I would like to thank the BYU College of Computational Mathematical and Physical Sciences for provided funding for these projects.

Contents

List of Figures

List of Tables

Chapter 1

Introduction and Background

This chapter introduces the core concepts that are used in the experimental work in this thesis. It begins by establishing the importance of directivity in musical acoustics and reviews relevant prior research. It then describes the structural vibration modes that influence how percussion and mallet instruments radiate sound. Finally, it introduces the concept of acoustic source centering, which is important for accurate directivity measurement and interpretation.

1.1 Introduction to Musical Directivity

In acoustics, directivity describes how the sound measured at a fixed distance from a source varies with angle relative to that source [8]. This property plays an important role in many applications, including spatial audio rendering, architectural acoustics, and musical acoustics. Directivity measurements offer insight into how sound sources radiate energy into their environments, which helps inform design decisions, microphone placement strategies, and modeling techniques.

Although previous research has extensively analyzed the directivity patterns of loudspeakers and other transducers [9–12], less attention has been paid to live sound sources. This is largely due to the difficulty of obtaining accurate and consistent measurements from sources such as speech

and musical instruments. Some of these challenges in directivity measurement were quantified in a capstone study by Denison [13].

Directivity is particularly important in musical acoustics because it reveals how sound disperses within performance spaces and influences how listeners perceive the sound field. Understanding these patterns informs performer placement, microphone design, and architectural decisions to create a more balanced and immersive listening experience.

The directional behavior of musical instruments is shaped by their design and structure. For example, string instruments such as the violin produce vibrations influenced by the instrument's body. This creates complex sound fields with varying directionality depending on frequency and playing technique [14, 15]. Percussion instruments are also greatly affected by their design. Drums produce sound by causing membranes to vibrate, which can create highly directional sound patterns [16, 17]. Wind instruments also exhibit complex directivity patterns due to their geometry and the way sound radiates from features like bells and open tone holes, often resulting in strong frequency dependence [18]. For example, brass instruments radiate omnidirectionally at low frequencies but become increasingly directional at higher frequencies due to the amplification from the bell [18, 19]. These design features determine the sound projection of an instrument, leading to various textures in musical performances, creating an interesting experience for the listener.

Some of the first efforts to measure and analyze instrument directivity began in the 1970s with the work of Meyer, who applied octave-band analysis in anechoic conditions using a loudspeaker and turntable setup with one microphone [18]. Cook and Trueman later investigated the directivity of six different string instruments using twelve microphones arranged around the source [1]. Otondo and Rindel extended this work to wind instruments using a circular array of thirteen microphones to produce polar plots of radiation patterns [2].

More recent studies have employed increasingly dense microphone arrays to improve spatial resolution. For instance, Pollow *et al.* used a 32-microphone spherical array to measure orches-

tral instrument directivity, although the array's resolution was limited at higher frequencies [20]. Hohlusing and Zotter advanced this approach with a 64-microphone spherical array that captured more detailed directivity patterns [3]. At Brigham Young University, Bodon renovated a high-resolution measurement system capable of capturing directivity for multiple sound sources [21]. Bellows later extended this platform, developing methods for acoustic source centering, optimizing microphone array sampling, and publishing a high-resolution open-source database of musical and vocal directivity data [22]. His work not only advanced centering theory but also contributed significantly to measurement quality and accessibility.

Figure 1.1 shows several measurement systems used in recent experiments, illustrating the progression from simple turntable setups to dense, automated arrays capable of capturing detailed acoustic radiation patterns. Unlike the BYU system, which captures repeated measurements across multiple angles for improved resolution and repeatability, most of these earlier setups collected data from a single fixed configuration or pass.

Capturing the directivity of musical instruments presents several challenges. These sources often radiate asymmetrically and with strong frequency dependence. Radiation may shift based on small changes in fingering, excitation force, or even body orientation [23]. Ackerman demonstrated that musical instruments can behave as dynamic sources, with radiation patterns that change in time due to player motion and evolving excitation conditions [23]. While Ackerman's work shows that musical instruments can behave as dynamic sources, this study focuses on stationary conditions to better understand the basic principles of how instruments radiate sound. Neither study includes the effects of the performer's body, which can influence the sound through movement or absorption. Exploring those effects could be a valuable direction for future work.

While these studies have significantly advanced our understanding of musical instrument directivity, many focus on individual instruments under idealized conditions. As a result, important factors such as mounting configurations, structural constraints, and register-dependent effects have

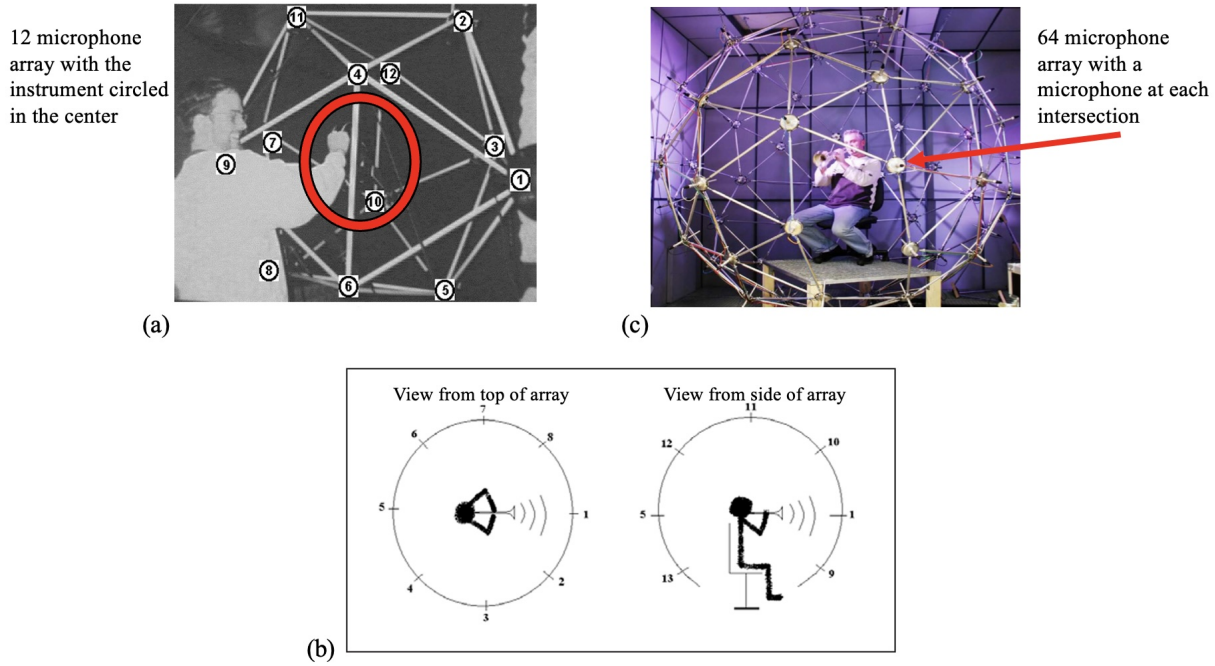

Figure 1.1 Directivity measurement setup from past musical acoustics experimentation. (a) Cook and Trueman, who used a 12-microphone array. Photo adapted from [1]. (b) Otondo and Rindel's circular array with 13 microphones. Photo adapted from [2]. (c) Photo adapted from Hohlusing and Zotter's 64 microphones in a spherical array [3].

received less attention. In particular, there is limited research on the directivity of percussion instruments in real-world setups and on how harmonic structure influences sound radiation in wind instruments. This research aims to address these gaps through targeted experimental studies.

1.1.1 Mode Shapes of Radiating Structures

The directivity of musical instruments is closely linked to their underlying structural vibration modes. For percussion instruments like drums, the primary radiators are circular membranes, while for mallet instruments such as the glockenspiel, each bar behaves approximately as a free-free beam.

Figure 1.2 shows the mode shapes of a clamped circular membrane. These mode shapes determine how the membrane vibrates and how sound is radiated into the surrounding air.

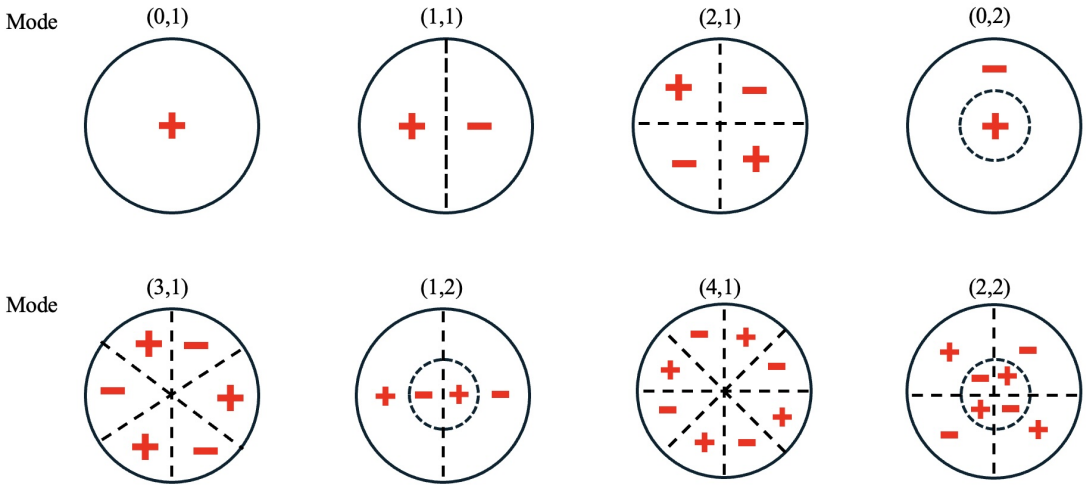

Figure 1.2 Mode shapes of a circular membrane. Modes are labeled by their number of nodal diameters and nodal circles.

Similarly, Figure 1.3 displays the bending mode shapes of a free-free beam, which approximates the behavior of individual glockenspiel bars. These bars radiate sound through transverse vibration, and their mode shapes influence not only the spectral content of the sound but also its directional characteristics.

Understanding these vibration modes provides valuable context for interpreting the directivity patterns measured in this work.

1.2 Introduction to Source Centering

Although directivity measurements provide valuable information on how sound is transmitted from an instrument, they are most accurate when combined with a clear understanding of the acoustic center of the instrument. The acoustic center is often defined as the point where spherical wavefronts begin to diverge [8, 24, 25]. In many cases, this acoustic center can shift depending on frequency, playing technique, or structural configuration [24]. For simple sources like loudspeakers, the acoustic center is typically fixed and well defined. But, for more complex instruments, especially

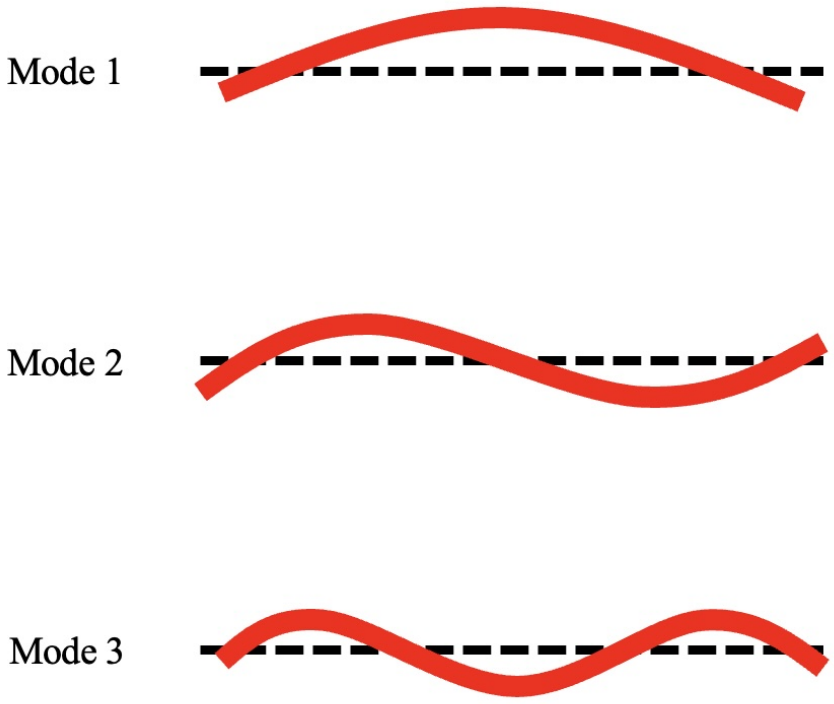

Figure 1.3 First three mode shapes of a free-free beam. These illustrate the bending modes that govern the vibration of glockenspiel bars.

those with multiple radiation points, such as the saxophone or percussion instruments, determining this center becomes more challenging.

The concept of source centering seeks to address this challenge by locating the position in space where wavefronts appear to diverge. When this point is known and used as the reference for directivity plots, the resulting data more accurately reflects the true radiation behavior of the instrument. Without proper centering, directional measurements can appear distorted or asymmetrical, potentially leading to inaccurate conclusions in applications like room acoustics modeling or instrument design.

Previous studies on acoustic centering have focused primarily on transducers and loudspeakers to improve the understanding of their radiation characteristics and optimize their design for various

applications. Some of these studies include finding the acoustic center of a laboratory microphone [26], and looking at the shift of the acoustic center in a loudspeaker when placed in a linear array [27]. Other studies have attempted to apply this to more complex systems, such as live instruments, with varying success due to the complexity of real-world radiation patterns [28].

Building on this foundation, Bellows conducted extensive work that significantly advanced the understanding of acoustic centering as it relates to musical instruments [22, 25]. His techniques were applied to a variety of instruments and helped in the creation of a comprehensive directivity database containing 16 different instruments. This work emphasized how important acoustic centering is in interpreting sound radiation and showed how it can be used to improve both measurement quality and acoustic modeling.

Despite recent advances, several aspects of source centering remain underexplored. For wind instruments, the acoustic center can shift across different registers due to changes in tone hole configuration and harmonic content, yet this behavior is rarely quantified. Similarly, the influence of structural supports or mounting conditions on the radiation patterns of percussion instruments has not been thoroughly investigated. These complexities highlight the need for further research that bridges the gap between theoretical centering concepts and the practical realities of musical performance.

1.3 Structure and Motivation

This thesis builds on the foundations of directivity and source centering and addresses key gaps in current literature. It consists of three main experimental studies, each organized as a standalone chapter:

- Chapter 2 investigates the directivity of several percussion instruments, including the bass drum, triangle, and open snare drum, in their mounted configurations. This addresses the

lack of data on real-world play settings and highlights how structural mounting influences radiation patterns.

- Chapter 3 focuses on the glockenspiel, combining vibrational analysis with directivity measurements. It explores how the bar's mounting impacts sound radiation, an area where prior studies have mostly focused on free-free bar conditions.

- Chapter 4 presents a harmonic and directivity analysis of the alto saxophone across three registers of the same pitch. This contributes new insights into how tone hole configuration and harmonic content influence radiation behavior, offering a better understanding of source centering in wind instruments.

The work presented in this thesis includes both original measurements and analysis performed by the author. For Chapter 2, the bass drum and open snare drum measurements were designed, conducted, and analyzed by the author using the high-resolution scanning system at BYU. The triangle measurement included in that chapter was performed by a previous BYU student; however, the data analysis and integration into this study were completed by the author. Chapter 3, which focuses on the glockenspiel, was carried out by the author. This work has been prepared for submission as an Express Letter for The Journal of the Acoustical Society of America. For Chapter 4, the alto saxophone measurements, source centering strategies, and harmonic analysis were also conducted and interpreted by the author. These contributions reflect a broad involvement in both experimental design and theoretical interpretation throughout the thesis.

By targeting these specific gaps, this work contributes to a deeper understanding of musical acoustics and provides practical tools for improving acoustic modeling, performance setup, and recording strategies.

Chapter 2

Directivity Analysis of Percussion Instruments

This chapter investigates the directivity of three percussion instruments, the bass drum, triangle, and open snare, using high-resolution, full-sphere measurements captured in the Directivity Measurement System at Brigham Young University. It details the experimental setups, excitation methods, and analyzes how design and mounting influence sound radiation patterns.

2.1 Introduction

As some of the oldest known musical instruments, percussion instruments have been essential to musical performance and cultural expression. Some of the first uses of percussion-like instruments were thought to be rattles, found in the Paleolithic era [29]. Over time, percussion instruments have evolved into the instruments we know today, such as the bass drum, cymbals, xylophone, and many more. These versatile instruments provide rhythm, texture, and timbre to a wide range of compositions and ensembles. Percussion has played an important role in human history, and until recently, the acoustic behavior of these instruments was often ignored. One of the most detailed

works on percussion acoustics was published by Fletcher and Rossing and covered many different classes of percussion instruments, including drums, mallet percussion, cymbals, gongs, bells, and many more [17]. The research advanced knowledge of many acoustic properties of percussion instruments, but it gave limited focus to characteristics like directivity.

Although directivity studies of musical instruments have become more common, percussion instruments are often overlooked in favor of strings, woodwinds, and brass. For example, the Audio Communications Group in Berlin created a database of directivity measurements for 41 musical instruments, but only two were percussion, and both were timpani [30].

Some studies have examined percussion instruments in more detail. Bellows, for instance, investigated the high-resolution directivity of gamelan gongs to analyze their low-frequency and nonlinear behavior [31, 32]. Other work by Pätynen and Lokki included measurements of timpani, bass drum, cymbal, and tam-tam as part of a broader orchestral directivity study [33]. However, their results do not offer high-resolution, full-sphere directivity data available in the current study.

Investigating the directivity of percussion instruments can improve our understanding of how these sources interact with performance spaces, contribute to ensemble balance, and impact recording practices. It also supports more accurate modeling and reproduction of percussion sounds in architectural acoustics and virtual environments.

This study examines the directivity of three percussion instruments: the bass drum, the triangle, and the open snare. Each instrument required slightly different experimental and analytical approaches, which are described in the following sections. Key goals include identifying frequency-dependent radiation behaviors, addressing measurement challenges such as repeatability and potential nonlinearities, and comparing narrowband and octave-band analysis methods. These results aim to advance our understanding of percussion acoustics and provide valuable data for performance, engineering, and acoustic research applications.

2.2 Bass Drum

2.2.1 Overview of Sound Radiation in Bass Drums

A fundamental concept of acoustics is the study of vibrational modes in circular membranes. One way these principles can be applied to real-world scenarios is through the circular heads of percussion instruments. Although these concepts do not apply to all instruments, they are useful when analyzing instruments such as cymbals, tambourines, and drums. With its large circular membrane, the bass drum is well suited for mode-based analysis. Building on this foundation, Fletcher and Rossing conducted studies on the bass drum that explored the vibrational modes of bass drums under varying head tensions and examined how their frequencies change after impact [17]. Fletcher and Bassett conducted another study that analyzed the acoustic properties of bass drum tones using 3-Hz band-pass filters to measure frequency, peak sound pressure, and decay rate from 40 Hz to 1000 Hz. They found that striking position affects the spectral emphasis, and synthesized tones based on measured components were nearly indistinguishable from real recordings in listening tests [34]. These studies helped to gain a better understanding of the bass drum's acoustic properties, but did not look at the directivity of the drum, which will be the focus of this section.

The bass drum is a fundamental percussion instrument, widely used across a range of musical genres to provide rhythmic and dynamic support. Its large size and construction contribute to complex radiation behaviors that are shaped by the interaction between the vibrating drumheads, the internal air cavity, and the surrounding environment [34]. Coupling between the batter (the struck head) and resonant heads plays a significant role at low frequencies, altering how sound is projected. Additional factors, such as location of the strike, tension of the drum head, and playing technique, further influence the acoustic output of the drum [17]. Understanding how a bass drum radiates sound is important for applications in performance acoustics, recordings, and instrument design.

This section explores the directivity of the bass drum through experimental measurement and analysis. Testing was conducted using a microphone array and controlled excitation methods to capture the spatial distribution of sound. The results highlight significant frequency-dependent variations in radiation and offer insight into how the directivity of the bass drum can impact musical acoustics and instrument setup.

2.2.2 Measurement and Data Collection Process

All measurements for the bass drum were completed in the large anechoic chamber at Brigham Young University. This chamber has a directivity measurement system (DMS) that features a 36-microphone array. The 180° arc array is designed to rotate a full 360°, with measurements taken at 5° increments. This results in 2521 different measurement points, providing a detailed characterization of the bass drum's directivity pattern. Due to the rotating nature of the array, this system is a repeated capture system, meaning a different measurement will be taken every time the microphones are rotated. This approach ensures that spatial variations in sound radiation are systematically recorded. A more detailed description of the DMS and its analysis techniques are available in [35, 36].

Since each data point is collected after rotating the microphone array, maintaining consistent excitation across all measurement positions is important. To ensure repeatability, an automated striking mechanism known as the thumper (Time Harmonic Undulating Mechanism for Percussion Excitation and Response) was used to strike the bass drum [37]. The thumper is a programmable device that delivers mechanical strikes with consistent timing, force, and contact location. Its design includes an adjustable mount that can hold multiple types of drumsticks, allowing users to match the playing implement to the specific instrument being tested. This approach minimizes variability caused by human performance factors such as fatigue, angle inconsistency, or off-center impacts.

Additionally, the thumper is mounted on a rigid frame to prevent unwanted movement and maintain precise alignment with the drumhead throughout testing. The system can be repositioned or reoriented as needed to strike different places on the membrane, such as the center or edge, depending on the test objective.

If a human performer were used to strike the drum for each of the 72 angular measurements, slight changes in force, position, or angle would introduce inconsistencies into the dataset. Furthermore, the presence of a person near the drum could reflect or obstruct sound waves, interfering with accurate spatial measurements. The thumper eliminates these issues, enabling precise, repeatable measurements that reflect the true radiation characteristics of the instrument. Figure 2.1 shows the bass drum and thumper setup.

Figure 2.1 The bass drum set in the DMS with the thumper set to its off-center strike position

Two sets of measurements were conducted to examine how striking position affects the bass drum's radiation characteristics. The first set involved striking the drum at the center of the head, while the second set used an off-center striking position. This was done to ensure that specific vibrational modes were not well excited by central excitation. Striking at the center primarily excites the drum head's axisymmetric modes, while off-center strikes can engage different modes by stimulating regions away from nodal lines. By capturing data from both striking positions, this study aims to provide a more comprehensive understanding of the bass drum's directivity and the role of excitation location in shaping its radiation patterns. Strike locations for this experimentation can be seen in Figure 2.2.

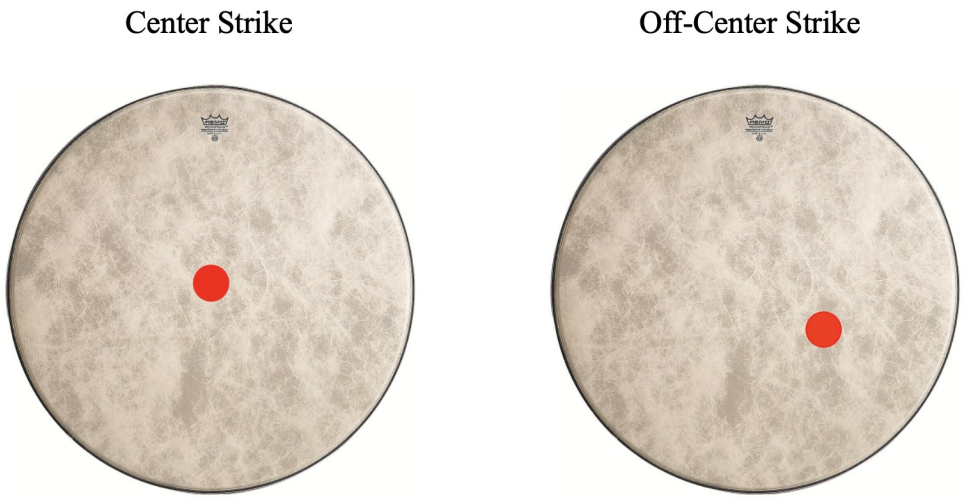

Figure 2.2 Strike positions of the two measurements shown on a bass drum head. Adapted from [4]

2.2.3 Results and Analysis

To analyze the directivity of the bass drum, both narrrowband and one-third octave band processing were applied, as shown in Figures 2.4 and 2.5. Each approach offers different advantages depending

on modal density and the complexity of the radiated sound field. The specific frequencies analyzed were selected based on prominent peaks in the power spectral density (PSD) plots (Figure 2.3). These peaks differ slightly between the centered and off-centered strikes because the excitation position influences which modes are most strongly excited. As a result, different frequency components emerge in each case, leading to the selection of narrowband peaks for further analysis.

When looking at the centered strike in 2.4, at low frequencies, where only a few strong modes are present, the results from both processing methods are similar. For instance, the narrrowband plot at 33 Hz and the 1/3 octave (OTO) plot at 31.5 Hz each show a clear dipole-like pattern aligned with the drumhead axis. This indicates that the energy in this range is dominated by a single mode, making either processing method equally effective.

As frequency increases, however, the differences become more pronounced. Around 63–70 Hz, the narrrowband plots begin to highlight subtle asymmetries and directional details, such as increased energy on the struck side, not as clearly visible in the broader OTO bands, which average energy across neighboring modes. This smoothing effect continues at 100 Hz and above, where narrrowband plots capture more localized modal contributions, while OTO plots yield more uniform patterns by blending multiple overlapping modes.

These distinctions are also evident in the off-centered strike results shown in Figure 2.5. At 35 Hz and OTO 31.5 Hz, both processing methods again show dipole-like behavior, confirming that modal spacing is sparse in this range. But at 60–63 Hz, narrrowband plots show more pronounced lobes near the striking point, while the corresponding OTO plot appears more balanced. At 122–125 Hz, where modal density increases, narrrowband plots reveal off-axis lobes and irregularities, while the OTO representation averages out these features into a more omnidirectional radiation field.

In general, narrrowband processing is ideal for isolating and analyzing individual modal behavior, especially when modes are well spaced. It offers high frequency resolution and is valuable for identifying the directional characteristics of specific frequencies. OTO analysis, on the other

hand, may be well suited for summarizing overall energy distribution, particularly in regions with high modal overlap, broadband content, or less predictable excitation, such as with percussion instruments.

Together, these methods provide a more complete picture of the drum's radiated sound. Narrowband plots support mode-specific interpretation, revealing detailed modal structures. In contrast, OTO plots are more relevant for practical applications such as room modeling, microphone placement, and performance setup because they better represent the broadband nature of real-world acoustic environments.

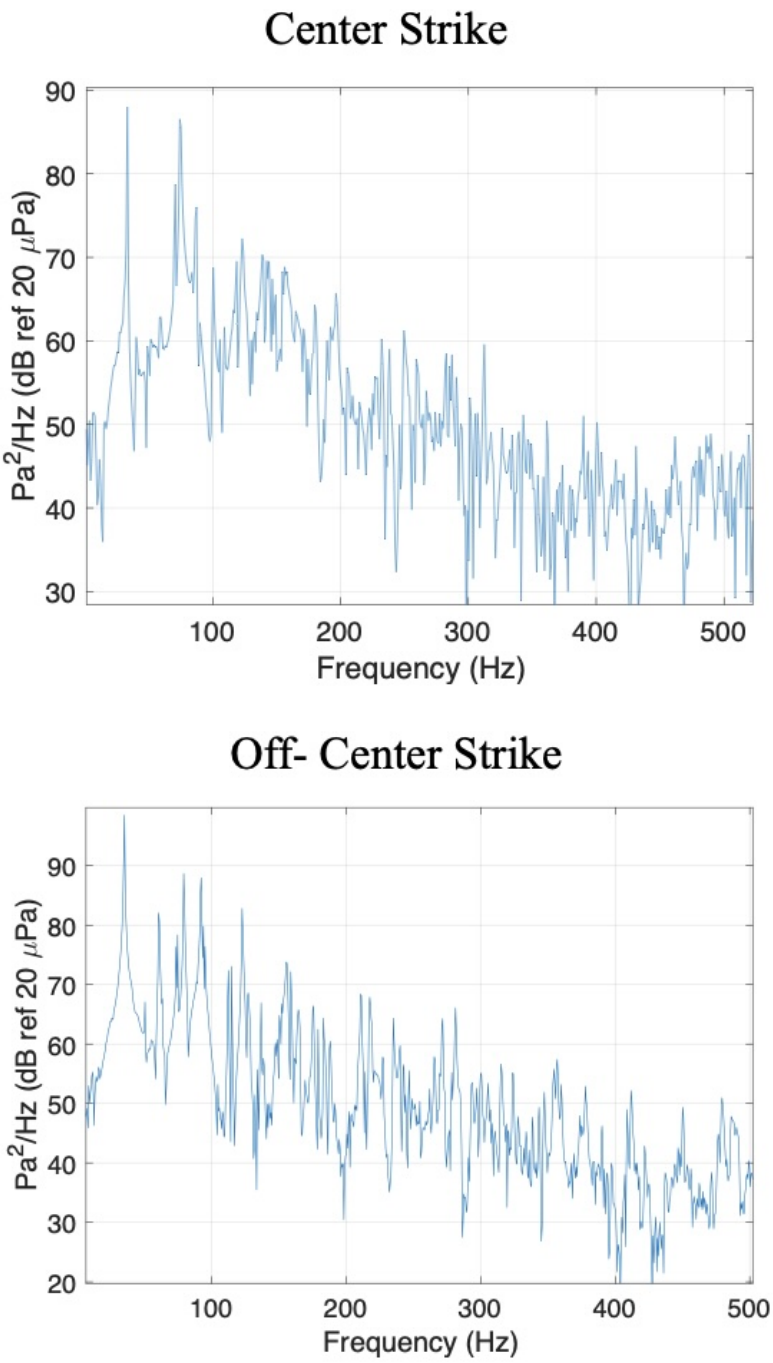

Figure 2.3 The power spectral density for the bass drum with two different strike positions. A few clear peaks are seen at low frequencies, but above 100 Hz, an increase in noise is seen.

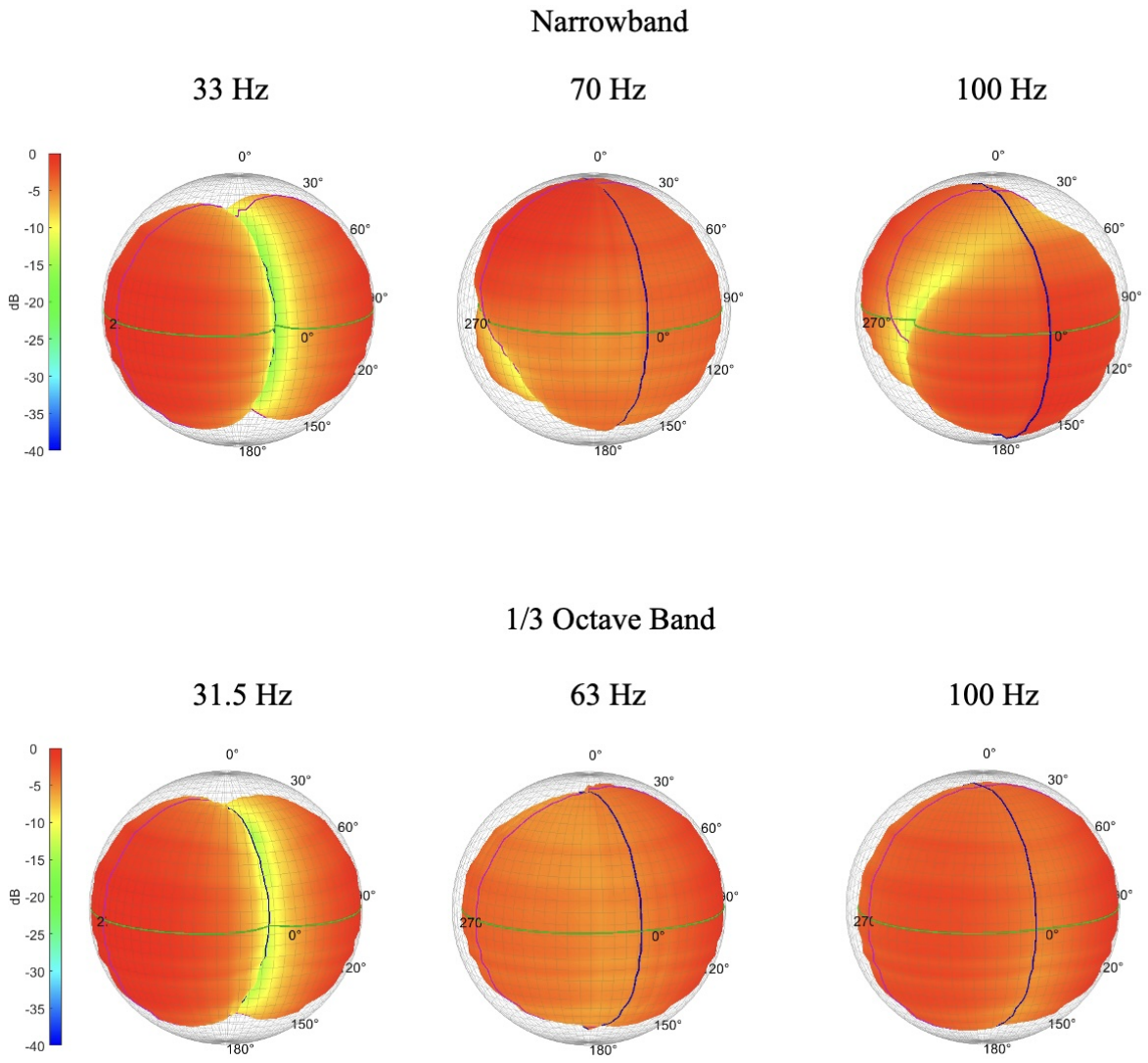

Figure 2.4 Directivity plots of the bass drum hit with a centered strike. The top row shows narrowband analysis, and the bottom row shows 1/3 octave band analysis.

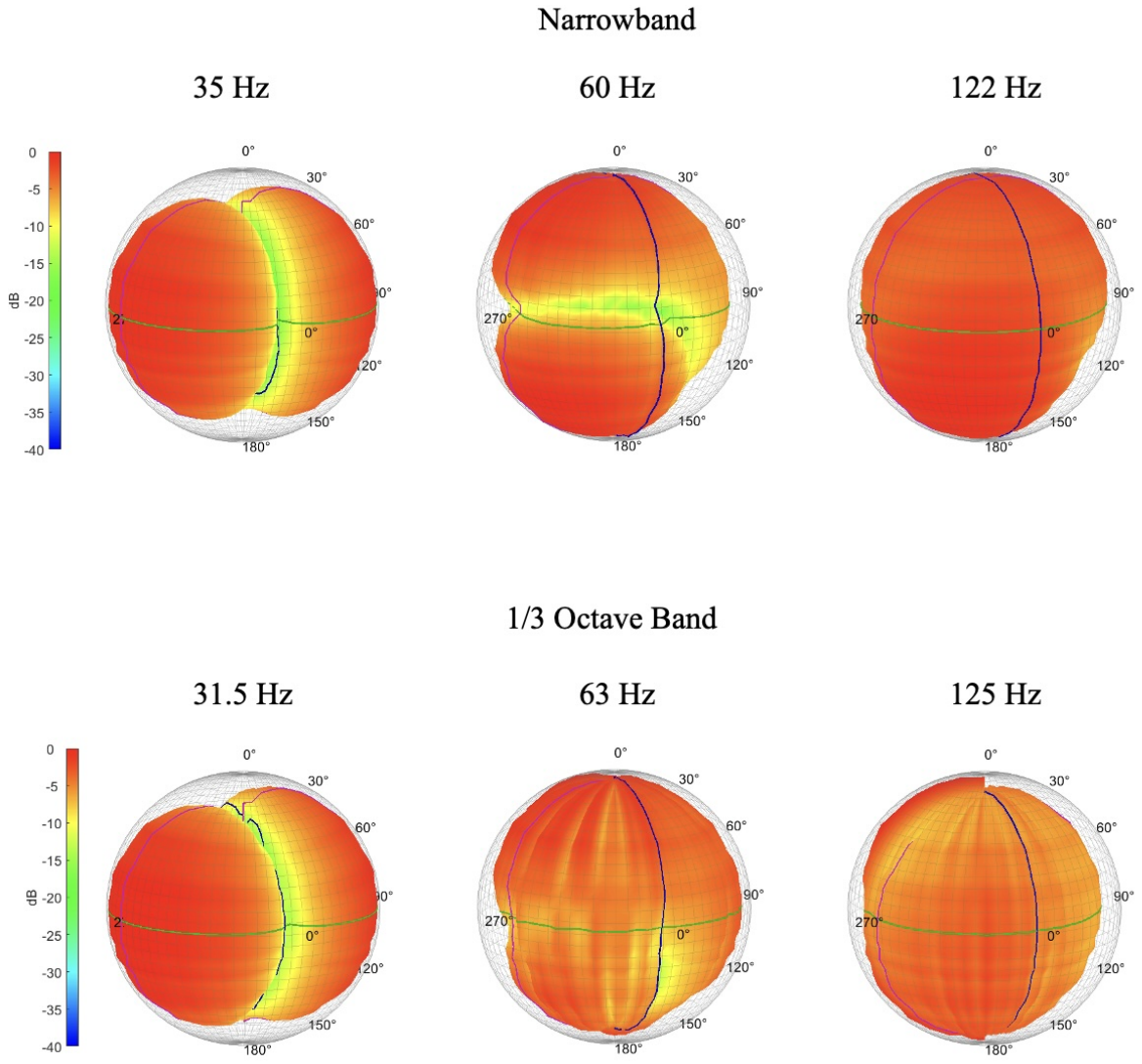

Figure 2.5 Directivity plots of the bass drum hit with an off-centered strike. The top row shows narrowband analysis and the bottom row shows 1/3 octave band analysis

2.3 Triangle

2.3.1 Overview of Sound Radiation in the Triangle

The triangle is a percussive instrument made by bending a metal bar into a triangle shape. It has distinct sound radiation properties due to the open-frame design and absence of a resonating cavity [38]. While drums or string instruments primarily use tensioned surfaces or air cavities to modify their sounds, the triangle uses its metal frame to convey sound. Previous research has shown that triangle bending modes maintain frequency characteristics similar to those of a straight bar of the same material and length before it is bent [38, 39]. More recent research has shown how aspects of the geometry of the triangle, such as the internal angle and the length of the side, can influence its frequency content [39, 40]. These studies provide useful background on the triangle's vibrational behavior, but aspects of its acoustic radiation, particularly directivity, are left unexplored.

The shape of the triangle has a large influence on its radiation pattern. Although circular or rectangular plates have clear vibrational modes, triangular frames support a combination of discrete and continuous vibrational modes [39]. The instrument is typically suspended by a string at one of its corners, creating a free-hanging configuration with minimal mechanical damping and long-lasting resonances [38]. When excitation or striking technique changes, so do the mode shapes and nodal points. These factors directly affect the strength and directionality of the radiated sound [39].

Understanding the sound radiation characteristics of the triangle is important for applications in musical acoustics, including microphone placement and virtual instrument modeling. By analyzing the directivity patterns of the triangle, researchers and sound engineers can optimize recording techniques and better predict how the instrument will blend within different performance environments.

2.3.2 Measurement Process and Directivity Analysis

The same directivity measurement system used for the bass drum was also used for the triangle, with minor adjustments to accommodate the instrument's open-frame geometry. Rather than being mounted to a platform, the triangle was suspended from a stand to simulate typical playing conditions and allow free vibration. Although a photo of the experimental setup was not available, Figure 2.6 shows a triangle similar to the one used in testing. A different excitation system was implemented for the triangle experimentation. The Scalable Automatic Modal Hammer (SAM) was used to deliver consistent and repeatable impacts, providing uniform excitation at each microphone position and reducing variability in the recorded data.

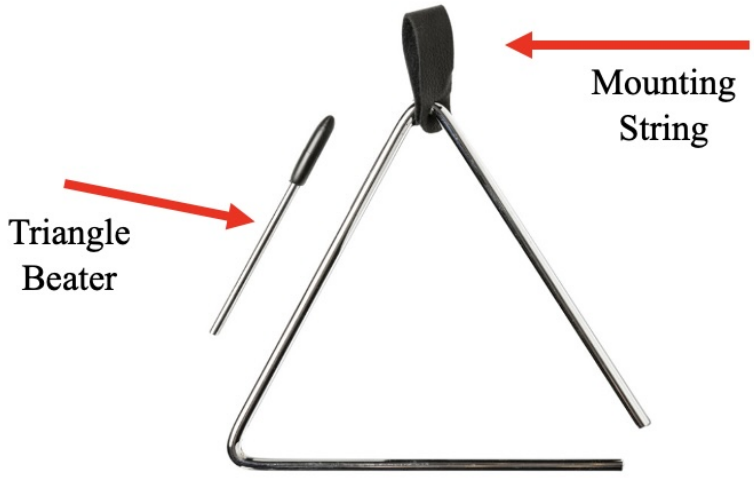

Figure 2.6 Triangle similar to the one used for directivity testing. The instrument was suspended from a string to allow free vibration. Image adapted from [5].

2.3.3 Results and Findings

A few key frequencies were selected based on the power spectral density shown in Figure 2.7. These specific frequencies were chosen because they show prominent lobing in the directivity pattern. Figure 2.8 shows the resulting directivity plots.

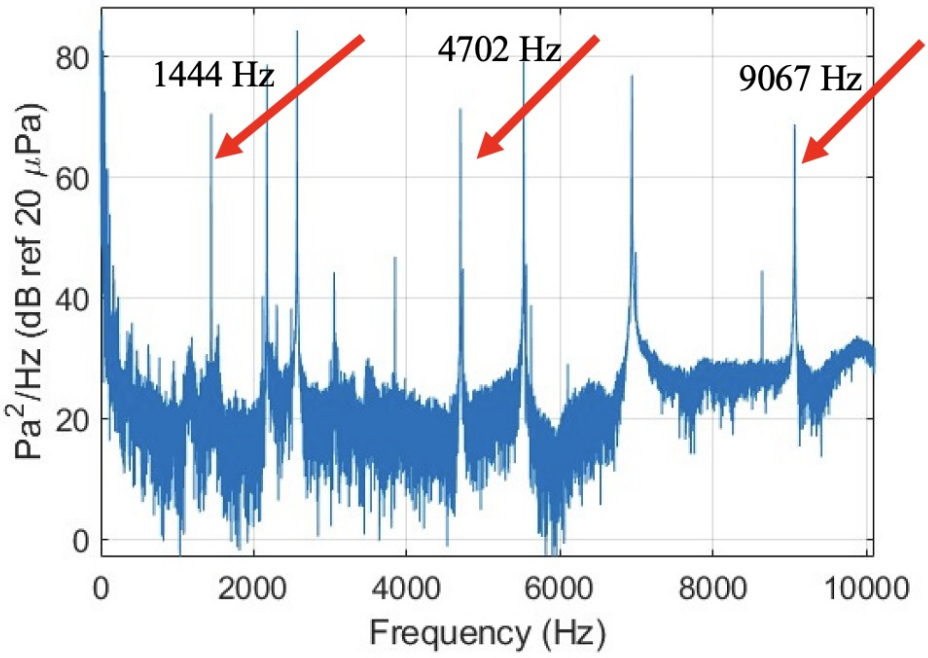

Figure 2.7 Power spectral density of a triangle, with peaks of interest pointed out with arrows.

At the fundamental frequency of 1444 Hz, four lobes emerge, primarily located near the corners of the directivity plot. There is a noticeable dip in radiation along the transverse and medial planes, with an even more significant drop directly at the center of the measurement. This may be due to interference in those directions caused by nodal behavior or equipment setup.

At 4702 Hz, the lobing becomes more defined. Six main lobes appear, and although the overall radiation is strong, small dips are visible within the lobes. The center of the plot again shows a reduction in radiation. The increased number and sharpness of lobes at this frequency likely

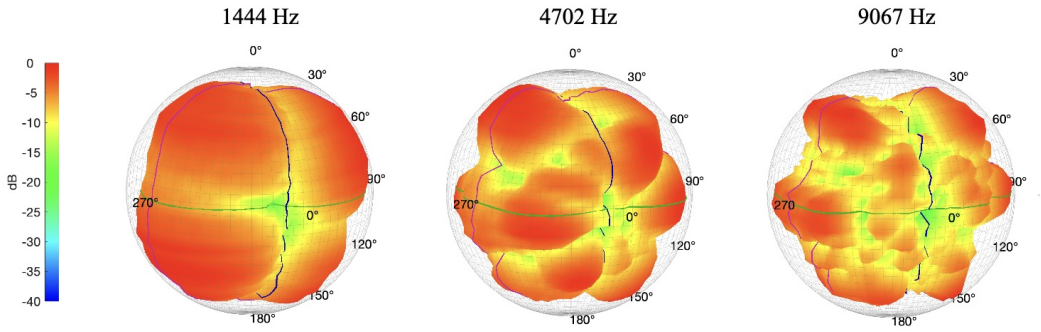

Figure 2.8 Directivity plots of the triangle at 1444 Hz, 4702 Hz, and 9067 Hz.

result from more complex vibrational modes being excited. These higher modes produce more directional radiation patterns, and the small dips within the lobes may indicate interference effects or asymmetries in how the triangle vibrates.

The six main lobes remain visible at the highest analyzed frequency, 9067 Hz, but are less pronounced than they are at 4702 Hz. The lobes are most distinct near the outer edges of the balloon plot, while the interior shows more irregular behavior. This could indicate a transition into higher-order modes, where the radiation becomes less coherent. As with the previous frequencies, there is a consistent drop in radiation at the sphere's center. This drop could potentially be due to mounting conditions of the equipment, such as the SAM.

2.4 Open Snare

2.4.1 Overview of Sound Radiation in the Open Snare

The snare drum plays a key role in many musical styles, known for its sharp attack and distinct articulation. Its sound is shaped by several factors, including shell construction, drum head interactions, and resonance within the cavity [41]. Understanding how the snare drum radiates sound is important for both performance and acoustic analysis.

When the snare wires are removed, the drum produces a more open tom-like sound. In this configuration, the batter head, the top head that is struck, and the resonant head on the bottom of the drum work together to shape the drum's sound [17]. Their interaction affects the timbre, sustain, and overall projection of the instrument. This interaction occurs most significantly at low frequencies and leads to the creation of mode pairs between the drum heads due to the acoustic and mechanical coupling [17]. The shell material, whether wood, metal, or acrylic, also affects the tone and resonance of the instrument, while the air vent can subtly change how the drum radiates sound [42].

Analyzing the directivity of an open snare drum helps better understand how its physical structure influences sound radiation. A detailed study by Rossing *et al.* used holographic interferometry, impulsive modal analysis, and accelerometer scanning to explore the vibrational modes of the snare drum, highlighting how the heads can move independently and produce complex mode shapes [43]. Their work focused on vibrational behavior, and this study builds on that foundation by examining the instrument's radiated sound field. Specifically, 3-D directivity plots will be used to visualize how sound spreads across space, offering a spatial perspective that complements existing mode shape research. This analysis also contributes to the broader study of percussion acoustics by showing how different instrument components work together to produce sound.

2.4.2 Experimental Setup and Data Collection

The setup and measurement process for the open snare drum followed the same general procedure as that used for the previous percussion instruments. The drum was raised on wooden blocks to allow the resonant head to vibrate, simulating typical playing conditions. However, this setup introduced a trade-off, as the blocks partially obstructed some of the radiated sound. The automatic striker, known as the thumper, was also elevated to accommodate a drumstick, ensuring that the excitation matched how a snare drum is typically played.

Figure 2.9 The open snare setup in the directivity measurement system. The drum is raised on wooden blocks to help simulate real-life playing conditions.

This setup is shown in Figure 2.9, where the snare is located at the center of the Directivity Measurement System (DMS). A full 4 pi space measurement was taken using the thumper to repeatedly strike the center of the batter head while the microphone array rotated in 5-degree increments. After the data were collected, an analysis of the directivity plots was done across a range of frequencies. These plots provided insight into how the open snare radiates sound, helping to visualize frequency-dependent changes in directivity patterns.

2.4.3 Results and Analysis

After data collection, the results were analyzed, and directivity balloon plots were produced at frequencies of interest that were determined from the power spectral density seen in Figure 2.10. The resulting balloon plots can be seen in Figure 2.11.

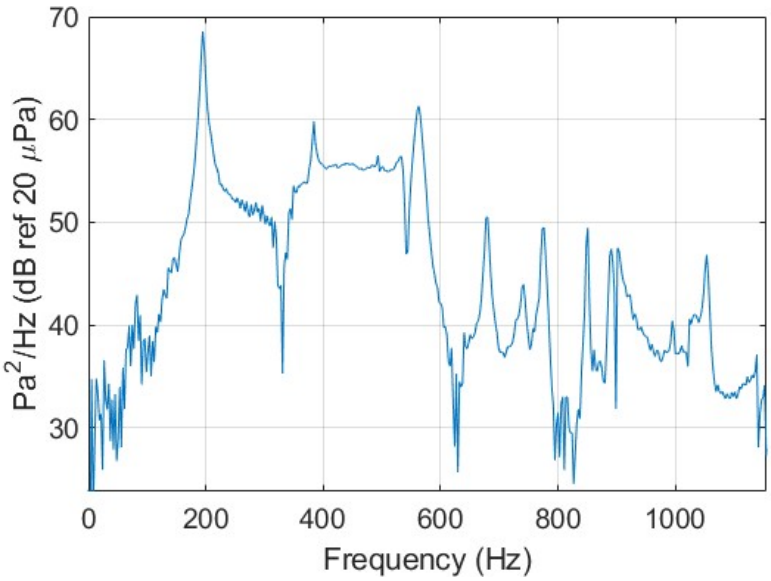

Figure 2.10 Open snare power spectral density with prominent peaks at 193, 380, and 562 Hz.

At the fundamental frequency of 193 Hz, the balloon plot begins to show characteristics of a dipole-like pattern. This may be due to the drumhead's first mode shape, where opposite sides of the membrane move out of phase, causing directional cancellation in certain directions. At 380 Hz, the radiation remains fairly even, but a more noticeable drop in radiation appears at the center of the plot. This could be due to the formation of more complex mode shapes on the membrane, where nodal lines limit sound radiation in specific directions. The deeper nulls in some directions may also result from physical obstructions in the setup, such as the striking device or reference microphone, interfering with the wavefronts. At 562 Hz, the radiation pattern becomes more uniform, showing the most omnidirectional behavior of the three frequencies. This could be attributed to higher-order

mode shapes exciting broader areas of the membrane, producing a more evenly distributed sound field. At this frequency, shorter wavelengths may also diffract more easily around the drum's structure, smoothing out directional variations.

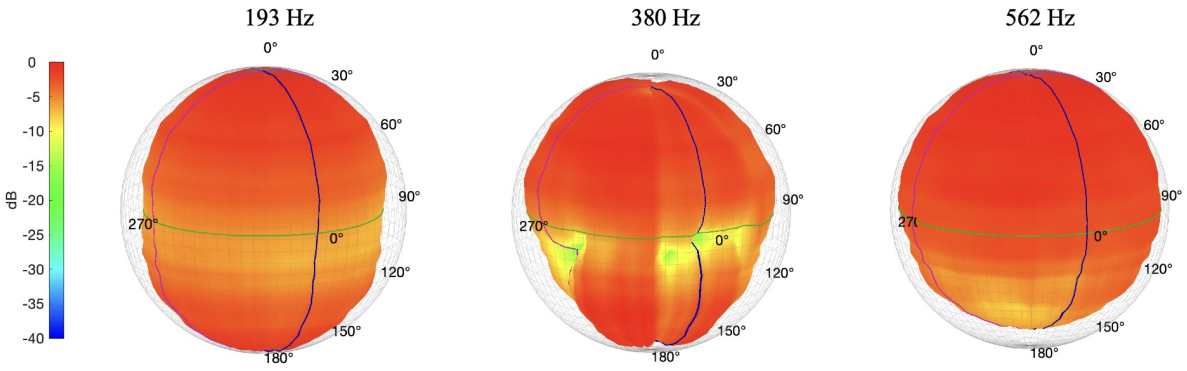

Figure 2.11 Directivity plots of the open snare at 193 Hz, the fundamental frequency, 380 Hz, and 562 Hz.

2.5 Conclusion

This chapter explored the directivity of three different percussion instruments: the bass drum, the triangle, and the open snare. Each instrument exhibited distinct radiation behaviors that reflect how it produces sound. The bass drum showed strong low-frequency dipole-like behavior that transitioned to omnidirectional spreading in the mid frequencies and eventually became more unpredictable at higher frequencies. Striking location also affected the radiation, with the off-centered strike producing slightly more asymmetric patterns. The triangle showed lobing at all frequencies and displayed a highly directional radiation pattern at higher frequencies, shaped by the complex vibrational behavior of its open-frame metal structure. Finally, the open snare showed dipole-like spreading at low frequencies, with some variation appearing in the mid-range, most likely due to cavity interaction, shell resonance, or potential equipment interference, and then omnidirectional spreading at higher frequencies.

The experimental setup and measurement process remained fairly consistent for each instrument. The variation in directivity reinforces how different physical configurations and excitation mechanisms affect sound radiation. These results highlight the importance of considering frequency content, structural design, and striking method when analyzing percussion instruments. There appears to be no existing literature that presents high-resolution, three-dimensional directivity data for the bass drum, triangle, or open snare using realistic excitation and mounting conditions. This type of information is useful for both acoustic modeling and practical applications like microphone placement in live and recorded settings. By visualizing how these instruments radiate sound in three dimensions, we better understand their acoustic output and the factors that shape it. The findings from this chapter contribute to the body of research on percussion instrument acoustics.

Chapter 3

Glockenspiel Directivity and Sound Radiation

This chapter looks at the vibrational and radiative properties of a glockenspiel bar in its mounted configuration and compares them to free-free beam behavior. High-resolution directivity measurements and scanning laser Doppler vibrometry were used to analyze how structural mounting influences sound radiation patterns and mode shapes. Supplementary materials, including detailed measurement data and additional figures, are provided in the appendices. These results help bridge the gap between theoretical models and the real-world acoustics of percussion instruments. This study has been prepared for submission to JASA Express Letters.

3.1 Introduction

The glockenspiel is a percussion instrument known for its bright, resonant tones, which has been an important part of orchestras and ensembles since its emergence in the 17th century [44]. It is constructed with metal bars arranged in a keyboard pattern, spanning two and a half octaves, made of approximately 30 to 34 steel bars with a length of 3.5 to 10 inches (8.9 - 25.4 cm) long [45].

There is no standard size for the glockenspiel, but most follow these dimensions. The bars are mounted in a wooden frame by resting on two thin mounting rails covered in felt. One end of the bar is attached to the rail with a screw while the other end is free to move. During normal playing configuration, the bars are not removed from the frame. The glockenspiel is typically played with hard plastic or wooden mallets that produce a bright, full sound [46].

Although this instrument is popular in many musical settings, the acoustics of the glockenspiel's bars, particularly within their mounted configurations, remain underexplored. Most research on glockenspiel bars has removed the bars from their original setups before testing, thereby idealizing them as free-free beams. While Fletcher and Rossing do not explicitly state that the bar was removed, their experimental approach and results suggest a free-free configuration [17]. This is supported by the work of Jones *et al.*, who clearly describe removing the bar and report similar results [47]. While such studies have provided valuable insights into the bars' natural frequencies and mode shapes, they do not account for mounting conditions that could affect the bars' motion. They also overlook how the bar radiates sound, which is a key factor in how both the performer and the audience hear the instrument.

Fundamental studies on the vibration and radiation of beams provide a useful foundation for understanding how musical bars behave acoustically. In particular, free-free beam models are often used to approximate the dynamics of metallophones like the glockenspiel. One important study in this area was conducted by W.K. Blake. His research focused on the radiation efficiency of free-free beams in air and water above and below acoustic coincidence [48]. In his study, the majority of bar modes occurred above coincidence, meaning that they radiated similar to a rectangular baffled piston. His work provides valuable insights for the glockenspiel with modes occurring above the coincidence frequency. Gaining a deeper understanding of the vibrational behaviors above coincidence is essential for interpreting the glockenspiel's acoustics.

This present study aims to expand on previous work that has been done with the glockenspiel by analyzing the bars in their mounted configurations using high-resolution directivity measurements and scanning laser Doppler vibrometry. Doing so helps address the gap in existing research by considering the practical constraints that influence the glockenspiel bars' vibrational and radiative properties. By preserving the instrument's authentic end constraints, the research offers a more accurate characterization of its acoustics. This approach helps improve theoretical understanding of the glockenspiel's vibrational behavior and also offers practical insights into its unique sound production. Ultimately, the work contributes to the broader field of musical acoustics by exploring the interplay between vibrational modes, mounting conditions, and sound radiation in the glockenspiel.

3.2 Methods

3.2.1 Directivity Measurement

The Directivity Measurement System (DMS) at Brigham Young University is a specialized setup designed to capture high-resolution spatial sound data of sound sources, including musical instruments [31,36]. The system consists of a 180° semi-circular array of free-field microphones spaced at 5-degree intervals, which rotates 360°. This configuration allows for over 2500 unique microphone positions, leading to a dense spatial sampling of the radiated sound field. In a typical measurement, the instrument or sound source is placed at the center of the array, and the microphones rotate around it. Because the system requires repeated captures at each angular position, the instrument must be struck or played multiple times to complete a full measurement.

To measure the directivity of a single glockenspiel bar (a D7), the bar was kept in its original frame in the glockenspiel and excited using an automatic striking device. The automatic striking device was designed to remotely and consistently strike the bar with a mallet, minimizing variation due to player fatigue or positioning [37]. Each strike was followed by a 10-second recording interval,

and then the microphone array rotated by 5° for the next measurement. This process was repeated 72 times, resulting in a complete spherical surface of acoustic data points. The purpose of this test was to identify which frequencies were excited in the bar and examine how the directivity patterns behaved at those frequencies. A more detailed description of the DMS and its analysis techniques is available in [35, 36].

Additional tests were conducted to isolate the influence of the glockenspiel frame and surrounding bars. These tests involved removing the bar from the glockenspiel and placing it in a 3D-printed mount made to simulate the conditions of the bar in the full glockenspiel without influence from the case and other bars. This allowed for direct comparison between the bar's behavior within the full glockenspiel and in isolation. The three testing conditions are seen in Figure 3.1.

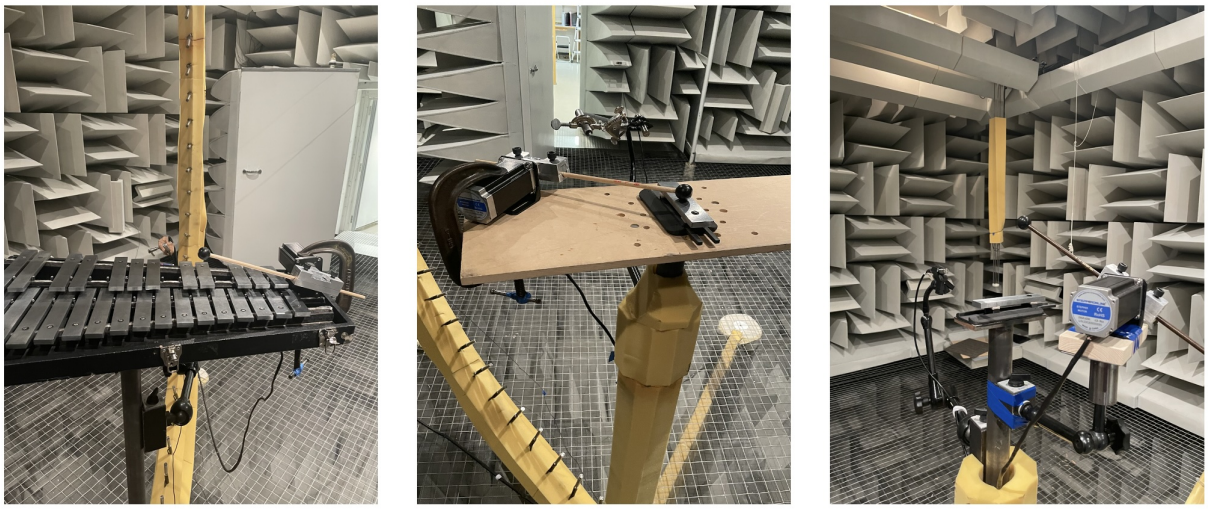

a) b) c)

Figure 3.1 Experimental setups for glockenspiel directivity measurements in the Directivity Measurement System at BYU. (a) Full glockenspiel with the D7 bar struck in place. (b) D7 bar mounted on a wooden board using a 3D-printed fixture. (c) Isolated D7 bar in the fixture without surrounding structure. The yellow rotating arm holds an array of microphones used for spatial capture.

3.2.2 Vibration Measurement

In addition to the directivity measurements, testing was also conducted using a scanning laser Doppler vibrometer. This provided high-resolution data on the vibrational modes of the glockenspiel bars. The purpose of this test was to analyze the vibrational characteristics of the glockenspiel, specifically the D7 bar, under different mounting conditions and at different frequencies.

To begin, the D7 bar was tested in its mounted position within the full glockenspiel. This setup allowed for an analysis of the bar's vibrational behavior while constrained in the way it is when played. The bar was excited by a speaker producing a sine sweep, and the resulting vibrations were recorded using the scanning laser Doppler vibrometer. After testing the D7 bar in its mounted configuration, the bar was removed from the frame to examine its behavior as a free-free beam. This was done to mimic the behavior of a simple beam and provide insight into the natural frequencies and mode shapes of the bar without external constraints.

The primary goal of this experimentation was to visualize the mode shapes of the D7 bar at different frequencies. These results were then used to compare the mode shapes and corresponding frequencies of the mounted glockenspiel bars with those of the free-free bar. The use of the scanning laser Doppler vibrometer allowed for measurements of the bar's displacement, producing operational shapes at the bar's natural frequencies, approximating mode shapes. This approach provided valuable insights into the differences in vibrational characteristics between the mounted and free configurations, offering a clearer understanding of how the glockenspiel's mounting influences the vibrational and radiative properties of the bars.

3.3 Results

3.3.1 Directivity Comparison

The following analysis focused on a single bar, the D7, which was made of steel and measured 5.6 × 1.3 × 0.4 inches (14.2 × 3.2 × 0.9 cm). The choice of using one bar was based on the assumption, supported by Fletcher and Rossing, that glockenspiel bars exhibit consistent mode shapes across different pitches [17]. As such, the insights gained from the D7 bar can be reasonably extended to other bars within the instrument.

Once directivity testing was completed, the data from the isolated bar and the full glockenspiel were analyzed. A power spectral density plot was created with peaks appearing at similar frequencies for both tests. The first three prominent peaks were analyzed, which occurred at 2374 Hz, the first bending mode, 6387 Hz, the second bending mode, and 7088 Hz, an unidentified mode which will be discussed in section 3.2. All three frequencies analyzed were above the critical frequency of the bar. These three frequencies were then used to produce the directivity balloon plots seen in Figure 3.2. Each row of the plot corresponded to a different test configuration with the glockenspiel bar. The top row shows the full instrument, the middle row shows the bar removed and placed on a large wooden board representing a small baffle, and the third row shows the bar removed with no surroundings. The boundary conditions for each configuration were considered the same since the 3D-printed mount accurately represented the rails of the wooden frame of the instrument. The orientation of the plots is shifted between the first two rows versus the bottom row due to a shifted array orientation during testing.

In the full glockenspiel configuration (top row), we observe that at lower frequencies, more acoustic energy radiates upward toward the top of the balloon, with less radiation directed downward. This trend is consistent across all frequencies in the full glockenspiel setup. At 6387 Hz and 7088 Hz, the downward radiation again diminishes significantly, by approximately 15–25 dB compared

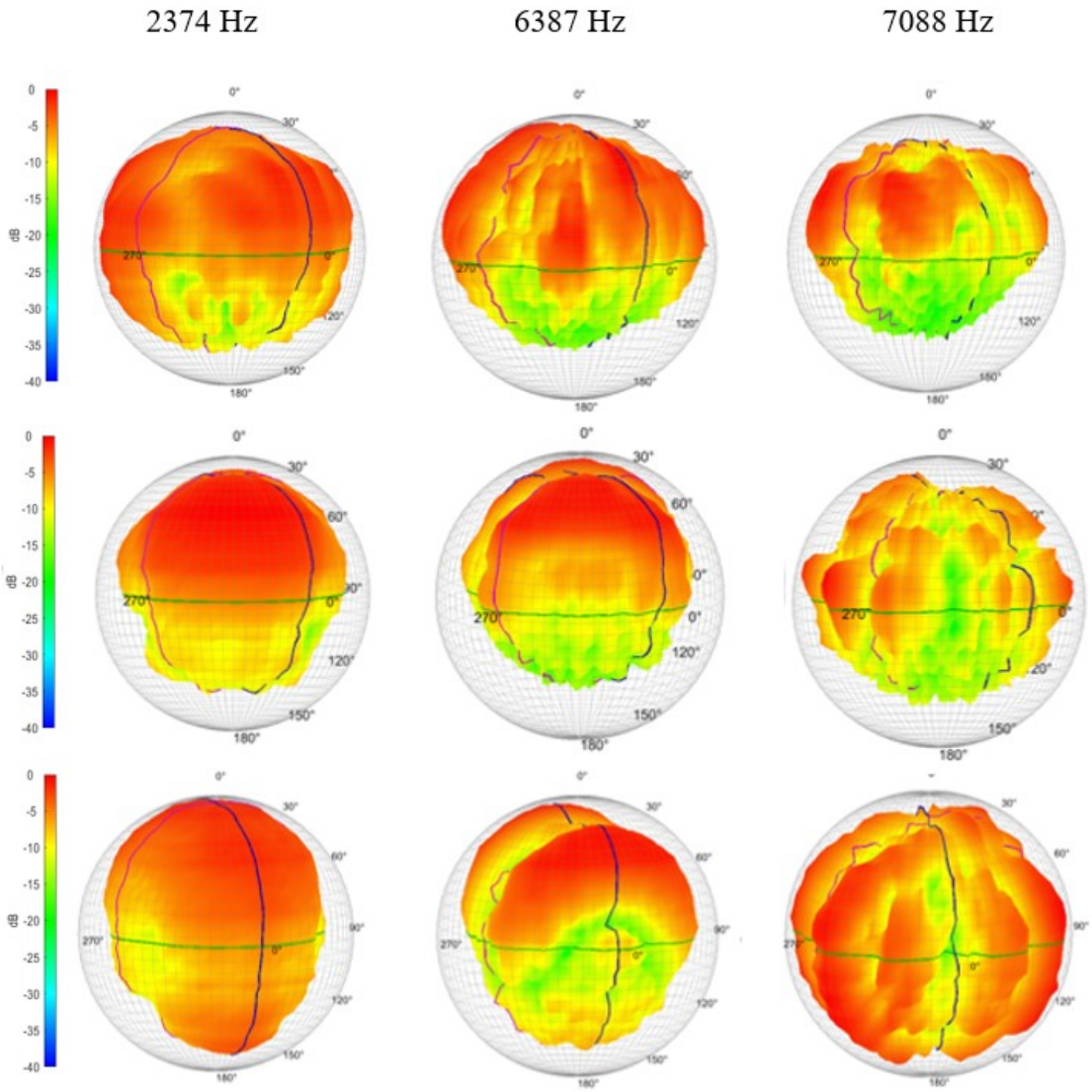

Figure 3.2 Directivity balloon plots for the D7 while in the full glockenspiel (top row), mounted on a board to simulate baffled conditions (middle row), and mounted in a 3-D printed fixture (bottom row). Red represents the maximum sound radiation, while blue represents 40 dB below the maximum.

to the upward and lateral directions. This drop is likely due to the shorter wavelengths at these frequencies, approximately 2.1 and 1.9 inches, which are more susceptible to interactions with the surrounding structure. These shorter wavelengths are more easily reflected or blocked by the glockenspiel frame and adjacent bars, limiting direct propagation of sound, particularly downward. In contrast, the fundamental's longer wavelength, about 5.7 inches, shows less attenuation (within 5–15 dB across directions), allowing for greater diffraction around obstacles and resulting in a more uniform radiation pattern. These observations highlight how the instrument's physical structure increasingly affects radiation as frequency rises.

In the baffled configuration (middle row), where the bar was mounted on a board using the 3D-printed fixture, a similar trend is observed. At 2374 Hz, radiation was again concentrated upward, with a drop-off below due to the board acting as a baffle. At 6387 Hz, stronger radiation occurs near the ends of the bar, at 0° and 180°, while a dip at the center may reflect nodal behavior or interactions with nearby structures. At 7088 Hz, the pattern becomes more irregular, with faint vertical lobes and a further decrease in downward radiation.

The isolated configuration (bottom row), with the bar mounted in the 3D fixture without a baffle, shows broader and more symmetric radiation at 2374 Hz. Although there is still a reduction along the sides of the bar (aligned with its length), this may be partially due to physical obstructions such as the striking device and reference microphone positioned along that axis, particularly near azimuthal angle 270°. At 6387 Hz, stronger radiation occurred near the ends of the bar, at 0° and 180 °, while a dip at the center may reflect nodal behavior or interaction with nearby structures such as measurement equipment. This end-focused radiation pattern shows qualitative agreement with the findings of Akay *et al.*, who observed similar lobing near the ends of beam-like structures following impact excitation [49]. At 7088 Hz, vertical bands of radiation appear uniformly across the sphere, with minimal difference between top and bottom, suggesting a more even radiation pattern between the top and bottom of the sphere at this higher frequency.

When comparing the radiation behavior across all three configurations, a few trends emerge. At 2374 Hz, all setups show similar strong radiation toward the top of the sphere. However, the full glockenspiel and baffled bar both show reduced downward radiation, supporting the conclusion that the instrument frame and surrounding bars introduce a baffling effect. As frequency increases, the baffled bar exhibits characteristics of both the full glockenspiel and the isolated bar. At 6387 Hz, it shows upward lobing similar to the isolated bar, while at 7088 Hz, its patchy radiation resembles that of the full glockenspiel. These comparisons reveal that each setup contributes uniquely to the resulting radiation patterns, and connections can be made to show that while the bar acts as a free-free beam, there are characteristics similar to a baffle coming from the glockenspiel.

3.3.2 Evaluation of Free-Free Bar Approximation

Previous studies by Fletcher and Rossing, and Jones *et al.* have suggested that glockenspiel bars behave similarly to free-free beams, with mode shapes and resonance frequencies that match theoretical predictions. These frequencies are summarized in Table 3.1 [17,47]. However, directivity measurements of the full glockenspiel revealed several resonance peaks that did not align with values reported in prior literature.

Power spectral density (PSD) analysis alone is insufficient for identifying mode shapes, as it only reveals frequency content without spatial information. To directly visualize the vibrational behavior, scanning laser Doppler vibrometry (SLDV) was used to capture the operational deflection shapes of the D7 glockenspiel bar at its natural frequencies. Two sets of measurements were performed: one with the bar suspended by fishing line to approximate free-free boundary conditions, and another with the bar mounted in the glockenspiel frame to represent realistic playing conditions. In both tests, the bar was excited using a MACKIE loudspeaker that swept through a range of frequencies, and the SLDV scanned a dense grid of points across the bar's surface. The free-free test used a 6×25 scanning grid, while the bar mounted in the glockenspiel was measured using a 5×23

grid. The resulting velocity fields were used to identify nodal locations and visualize bending and torsional mode shapes. The roughly 6 mm spacing of the SLDV scan dictates that the accuracy of node line estimates is less than 3 mm. The free-free scans showed strong agreement with classical beam theory predictions from Kinsler *et al.* [50], while the mounted case revealed how structural constraints influenced the vibrational response. These comparisons are illustrated in Figure 3.3.

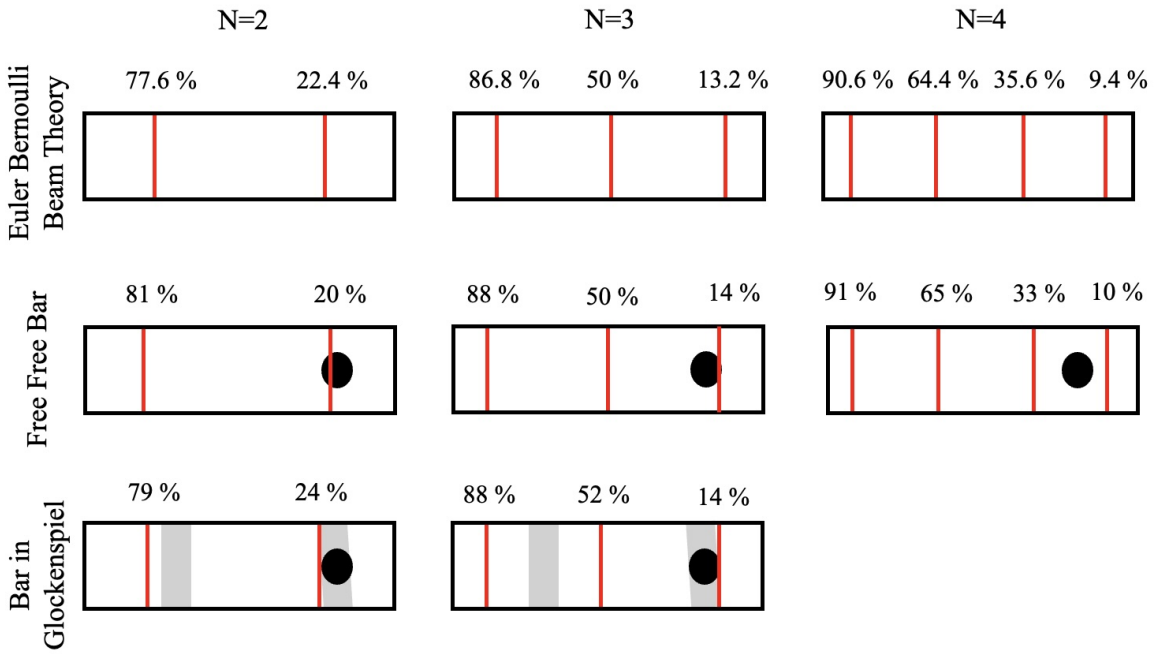

Figure 3.3 A comparison of the analytical/estimated nodal positions (shown as red lines) for the first three bending modes of a beam. Theory is compared to a free glockenspiel bar and a glockenspiel in the full setup. There were inconclusive results for the bar in the glockenspiel when N=4. The thick gray bars represent the wooden rails of the glockenspiel frame.

For the first bending mode, the predicted nodal positions for a free-free bar, based on Euler-Bernoulli theory, were at 22.4% and 77.6% of length of the bar. Experimental measurements on the free-free bar aligned well, showing nodes at 21% and 81% of the length. The glockenspiel bar mounted in its frame exhibited nodes at 24% and 79% of the length, which were close to the

predicted values. These minor deviations may be attributed to the effects of mounting constraints, added mass from suspension points, or the mounting hole. An important detail shown in Figure 3.3 is that the bottom mounting pad on the glockenspiel bar does not rest at a nodal location for the first bending modes. While the measured nodal positions are still in good agreement with theory, this off-nodal support may help explain some of the small discrepancies observed between the free and mounted configurations. Additionally, the exact symmetry of the nodal lines is disrupted by the presence of the mounting hole, which alters the mass and stiffness of the bar.

In the second bending mode, theoretical nodal locations were expected at 13.2%, 50%, and 86.8% of the bar length. The free-free bar had nodes that shifted slightly from expected values, at 14%, 50%, and 88%. The glockenspiel bar displayed similar nodal positions at 14%, 52%, and 88%, suggesting that frame interaction may have an effect at higher modes, most likely due to increased sensitivity to boundary conditions. Overall, the measured values were in general agreement with the predicted values.

The nodal points were predicted at 9.4%, 35.6%, 64.4%, and 90.6% of the length for the third bending mode. The free-free test measurements showed similar measurements, with nodes at 10%, 33%, 65%, and 91%. However, data for the full glockenspiel bar at this frequency were inconclusive due to unclear scan results. This may be addressed in a future study.

Overall, the bar set in free-free conditions and mounted glockenspiel bar showed strong agreement of nodal positions with Euler Bernoulli beam theory for the bending modes of the bar. There are slight discrepancies between node positions, most notable at the second bending mode, which highlight the influence of real-world mounting and construction on vibrational behavior.

Table 3.1 compares measured modal frequencies of the D7 bar to values reported in the literature and to theoretical predictions. Measurements were taken under two configurations: a free-free setup, where the bar was suspended using fishing line, and a mounted setup, where the bar remained in the full glockenspiel frame. In both cases, the bar was struck with a mallet to mimic typical

excitation. As a note, we follow the convention of denoting the fundamental bending mode as N=2 as seen in the Hambric tutorial [51], though other conventions have also been used. While the bending modes generally show good agreement with previous work and theoretical beam models, torsional modes deviate more substantially. These discrepancies may stem from differences in excitation methods, the influence of the mounting hole on stiffness distribution, and the simplifying assumptions inherent in beam theory.

Torsional mode predictions from Garrett [52] were more consistent with measured glockenspiel frequencies than those from Fletcher and Rossing or Jones *et al.* One torsional mode not reported in earlier studies matched closely with Garrett's theoretical values, supporting the idea that more detailed models may be necessary to predict torsional behavior. Percent errors for torsional modes were as low as 2.8% with Garrett's predictions, while other literature sources differed by up to 47.8%. These discrepancies likely stem from simplified torsional theory, which does not account for warping or the coupling between bending and shear forces, effects that become more influential at higher frequencies [53]. There is also the potential for rotary inertial effects causing the mismatch.

Finally, additional peaks in the power spectral density were observed at 7088 Hz and approximately 16,000 Hz, but only when the bar was struck with an impact rather than excited by the speaker. These peaks appeared consistently in both the free-free suspended configuration and when the bar was mounted in the full glockenspiel. Although these frequencies did not correspond to clearly identifiable modes, vibrometer scans revealed motion patterns that loosely resembled high-order bending modes. As a possible explanation, the longitudinal mode frequencies of the bar were also considered. However, the first longitudinal mode is predicted to occur at approximately 17,769 Hz, significantly higher than the observed peaks, making it an unlikely source. Determining the precise cause of these responses would require further investigation, but such analysis falls outside the scope of this study.

Table 3.1 Comparison of experimental and published mode frequencies. Percent errors are shown in parentheses and are calculated against the free-free glockenspiel bar strike test. All units are in Hz.

Mode	**Free-Free**	**Full Glockenspiel**	**Fletcher & Rossing**	**Jones *et al.***	**Euler-Bernoulli**	**Garrett**
Fund. (N=2)	2367	2374	–	–	–	–
Torsional	$F_1 \times 2.41$ $= 5711$	$F_1 \times 2.41$ $= 5740$	Not Present	Not Present	–	$F_1 \times 2.34$ $= 5555$ (2.8%)
Bend (N=3)	$F_1 \times 2.69$ $= 6375$	$F_1 \times 2.69$ $= 6387$	$F_1 \times 2.71$ $= 6414.57$ (0.6%)	$F_1 \times 2.8$ $= 6627.6$ (3.8%)	$F_1 \times 2.756$ $= 6523.45$ (2.3%)	–
Nonstandard Mode	$F_1 \times 3.01$ $= 7129$	$F_1 \times 2.98$ $= 7090$	Not Present	Not Present	–	–
Torsional	$F_1 \times 4.87$ $= 11,547$	$F_1 \times 4.88$ $= 11,596$	$F_1 \times 3.57$ $= 8450.19$ (36.6%)	$F_1 \times 3.3$ $= 7811.1$ (47.8%)	–	$F_1 \times 4.7$ $= 11,111$ (3.9%)
Bend (N=4)	$F_1 \times 5.07$ $= 11,997$	$F_1 \times 5.06$ $= 12,015$	$F_1 \times 5.15$ $= 12,190.05$ (1.5%)	$F_1 \times 5.1$ $= 12,071.1$ (0.6%)	$F_1 \times 5.404$ $= 12,791$ (6.2%)	–
Nonstandard Mode	$F_1 \times 6.9$ $= 16,341$	$F_1 \times 6.85$ $= 16,268$	Not Present	Not Present	–	–
Torsional	$F_1 \times 7.46$ $= 17,652$	$F_1 \times 7.46$ $= 17,715$	$F_1 \times 7.07$ $= 16,734.69$ (5.5%)	$F_1 \times 6.1$ $= 14,438.7$ (22.3%)	–	$F_1 \times 7.04$ $= 16,666$ (5.9%)

3.4 Conclusion

This study examined the acoustics of the glockenspiel by analyzing its vibrational and radiative properties in a mounted configuration, addressing a gap in previous research that often only considers the modes of free-free beams. Directivity measurements and the scanning laser Doppler vibrometer were used to assess how the glockenspiel's unique mounting conditions influence its vibration and sound radiation. The results indicated that the entire glockenspiel behaves differently compared to an isolated single bar, with evidence of baffling effects and reflections from adjacent bars and the instrument case. These things influence the radiation patterns, most notably at higher frequencies where diffraction effects become more evident.

Additionally, a comparison between the measured vibrational modes and traditional free-free beam models showed that while the bending modes align reasonably well, differences in torsional modes suggest that the free-free approximation does not fully capture the behavior of the mounted bars. The identification of unexpected spectral peaks further supports the need for a more refined model that accounts for the constraints imposed by the instrument's frame.

By maintaining the regular mounting conditions of the instrument, this research provides a more accurate characterization of the glockenspiel acoustics, offering insight for both theoretical modeling and practical applications in instrument design and performance. Future work could explore the role of case resonances and interactions between adjacent bars to further refine our understanding of the sound radiation of the glockenspiel.

Chapter 4

Harmonic Analysis of the Alto Saxophone

This chapter explores how the harmonic structure and sound directivity of the alto saxophone vary when playing a B flat in three different registers. The experimental setup used to collect directivity and spectral data is described, followed by an analysis of the harmonic content and directional sound radiation for each register. Balloon plots and spectral comparisons are used to highlight how changes in register influence the distribution of radiated sound.

4.1 Introduction to Source Centering and Directivity in Wind Instruments

Understanding how sound radiates from an instrument begins with the concept of the acoustic center, the point from which spherical wavefronts seem to diverge [8,24]. This location is identified through a process known as source centering. Accurate source centering is essential for applications such as directivity measurements, where directional sound patterns depend on identifying the effective origin of radiation. It also plays a crucial role in improving acoustical models used in instrument design, sound reproduction, and room acoustics.

Source centering becomes especially important for musical instruments with non-uniform or frequency-dependent radiation characteristics. In such cases, the acoustic center can shift based on pitch, dynamics, or structural changes [24, 54]. By understanding this behavior, researchers can better predict sound behavior and optimize recording and sound reinforcement techniques.

This complexity is further amplified in wind instruments, where different notes are produced by opening and closing various combinations of tone holes. Since these tone holes act as the primary radiators, the location of the acoustic center shifts with each fingering configuration. In addition, because multiple harmonics are present in any played note, the effective acoustic center at a specific frequency may depend not only on frequency itself, but also on which note is being played. This frequency-dependent behavior introduces significant challenges for directivity measurements and modeling.

Previous large-scale efforts, such as the acoustic radiation pattern database by Shabtai *et al.* [28], provide valuable baseline data for 41 instruments, including the saxophone. However, this database uses one-third octave band smoothing, which limits the resolution needed to analyze harmonic structure and register-specific directivity.

To begin addressing these gaps, a more targeted investigation is needed—one that explores how the directivity of a single pitch varies across registers. The present work contributes to this effort by analyzing how tone hole configuration and harmonic structure affect radiated sound.

To begin addressing this complexity, a more foundational study is needed that examines how the directivity of a single pitch varies across different registers. The present work contributes to this effort by analyzing how tone hole configuration and harmonic structure affect radiated sound.

4.2 Saxophone Directivity Across Registers

This chapter investigates how the directivity and harmonic structure of the alto saxophone change when playing a B flat in three different octaves, B flat 3, B flat 4, and B flat 5, using transposed (alto saxophone) pitch notation throughout. While each note is a B flat, they differ in register and frequency, resulting in distinct radiated sound fields. These differences arise from changes in harmonic content and the configuration of open tone holes along the instrument's body.

When the saxophone is played, sound radiates primarily from any open tone holes and somewhat from the bell. The alto saxophone has 25 tone holes, and depending on the fingering, the radiation pattern can shift [55]. For example, when a low B flat is played, almost all tone holes are closed, and sound is expected to radiate primarily from the bell. In contrast, when playing a middle or high B flat, more tone holes are open, shifting the primary radiation source upward from the tone holes along the body of the instrument. Figure 4.1 illustrates the fingerings for all three B flats, showing the increase in open tone holes with register. Figure 4.2 shows the expected change in radiation source location: upward and outward from the bell for the low B flat, and from higher along the tone hole openings for the middle and high B flats.

Another significant factor influencing directivity is the harmonic structure of the note. The harmonic differences that are present with each B flat interact with the bore geometry and tone hole layout, shaping how sound is radiated [55]. In higher registers, differences in playing technique and fingering can emphasize certain harmonics over others, leading to noticeable changes in the overall radiation pattern.

While harmonic structure and tone hole configuration play a major role in shaping directivity, previous research has also investigated other acoustic properties that contribute to the saxophone's complex radiative behavior. Luchetta *et al.* used acoustic modal analysis to extract resonance frequencies and cavity mode shapes of a tenor saxophone, demonstrating the influence of mouthpiece volume and providing a framework for validating numerical models [56]. Benade and Lutgen

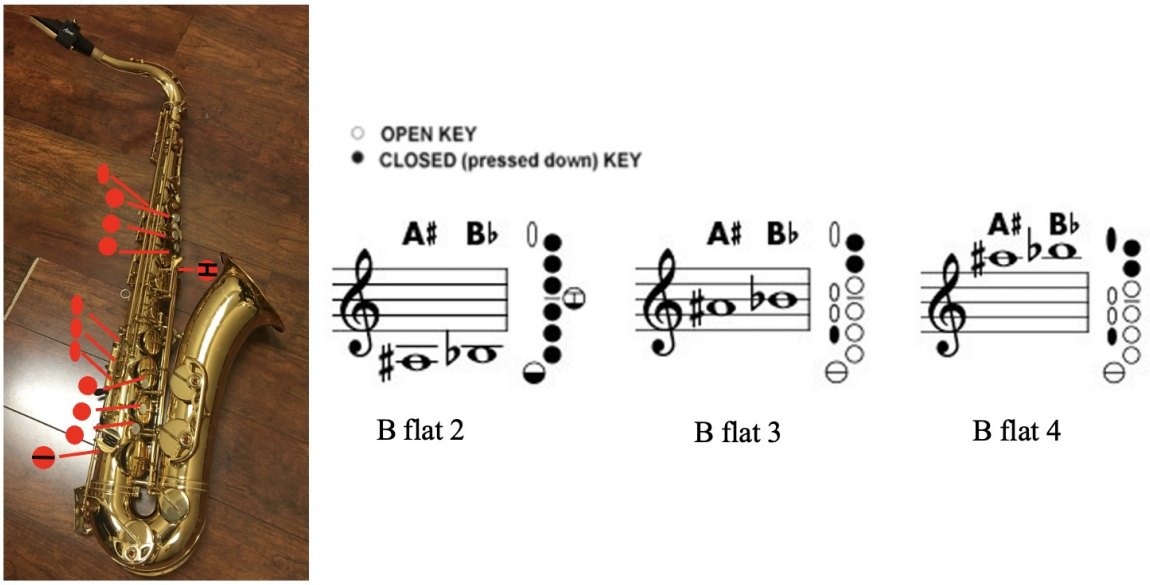

Figure 4.1 Custom alto saxophone fingering chart adapted from [6]. Black circles indicate keys that are pressed (closed), and white circles indicate keys that are unpressed (open). The left image shows the physical saxophone with key locations, while the three diagrams to the right show standard notation and corresponding fingerings for the low, middle, and high B flats (from left to right).

performed spectral measurements across most notes in the low and second registers of alto and tenor saxophones, finding that the spectra followed a consistent envelope defined by a characteristic break frequency tied to the tone hole lattice cutoff [57]. Their work explained spectral roll-off and notches caused by reed beating, aligning well with theoretical models.

Further studies have examined the internal acoustics of the instrument. Ukshini and Dirckx mapped the sound pressure along the saxophone bore and found that the cutoff frequency varies with register and fingering, often occurring at lower modal positions than previously assumed. They also showed that register valves significantly impact the sound pressure distribution within the bore [58]. Petersen *et al.* extended cutoff frequency theory to conical instruments, showing that saxophone tone hole lattices are acoustically irregular and that cutoff frequency decreases across the first register from high to low notes [59].

Figure 4.2 Expected radiation paths for the low B flat (left) and middle/high B flat (right). Red arrows illustrate the general direction of primary sound radiation based on tone hole configuration. These arrows are intended to provide a conceptual visualization and are not drawn to represent precise angles or magnitudes. Alto saxophone image adapted from Schmitt Music [7]

Additionally, researchers at the University of New South Wales have conducted extensive experimental and theoretical studies on saxophone acoustics. Their work includes detailed measurements of input impedance, resonance frequencies, and sound spectra across various fingerings and dynamics. They highlight the significance of cutoff frequencies, impedance peaks, and the influence of register holes and bell flare on tone production. These resources provide one of the most comprehensive acoustic mappings of the saxophone available in the field.

Together, these studies provide a broad understanding of saxophone acoustics, highlighting how structural and spectral properties shape sound production. The present work contributes to this effort by examining how tone hole configuration and harmonic structure influence radiated sound in a spatial context, offering new insight even without directly computing the acoustic center.

By comparing the directivity of the alto saxophone for three different B flats, this study aims to better understand how register and instrument configuration affect sound radiation. Each B flat involves a different tone hole configuration, which in turn influences the location and behavior of the primary radiating sources. Although this work does not explicitly compute the acoustic center, the resulting directivity data provide insight into how the effective source location shifts with register, an important consideration in source centering. Understanding these register-dependent changes can inform practical applications such as microphone placement, spatial audio design, and instrument modeling.

4.3 Experimental Methods

Testing was conducted in the anechoic chamber at Brigham Young University using the Directivity Measurement System (DMS). A saxophonist was positioned at the center of a 180° arc, 36-microphone array as seen in Figure 4.3. The player was seated 3 feet above the chamber's wire floor to align the bell of the instrument with the center of the array. A laser was shined at the instrument to keep the location as consistent as possible for each measurement. A tuner was also used to keep the pitch within 5 cents sharp or flat of the fundamental frequency of the note. A low B flat, at 138 Hz, was played for 10 seconds, and then the microphone array was rotated in 5° increments. This process was repeated until a full 4 pi space dataset was collected. Additional details about DMS instrumentation, data capture, and processing can be found in [35, 36].

Additional tests were performed using the same procedure for the middle B flat, an octave above, at 277.2 Hz, and two octaves above at 554.37 Hz. Comparing the directivity patterns across these notes provides insight into how the location of the primary radiating source changes with register. This phenomenon, known as source centering, describes how the effective acoustic center of radiation changes depending on which tone holes are open. Observing this behavior across

Figure 4.3 Saxophone setup in the DMS, with the player raised 3 feet above the ground.

octaves provides valuable insight into how the location and shape of the radiated sound field change. Understanding this relationship contributes to a more complete characterization of saxophone acoustics.

4.4 Results and Analysis

4.4.1 Harmonic Content Analysis

To better understand how the harmonic structure contributes to the differences in directivity between the registers, the spectral content was analyzed for each of the three B flats. The pressure signal at

270°, directly in front of the saxophone, was studied. This angle was chosen because it was a point of strong radiation for all three notes and provided a consistent comparison point. The spectra were plotted up to 2500 Hz, and harmonic peaks were compared across registers as seen in Figure 4.4.

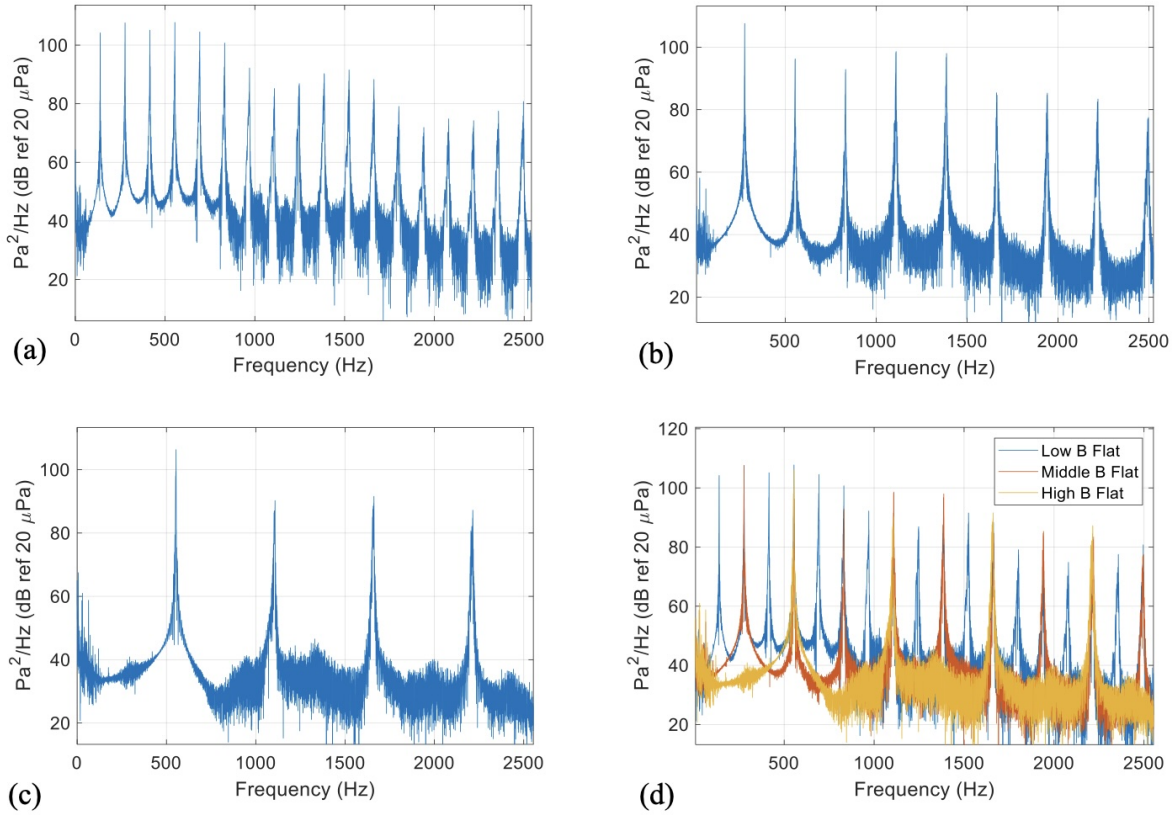

Figure 4.4 Power spectral densities (PSDs) for the alto saxophone playing B flat in three registers. (a) Low B flat, (b) middle B flat, and (c) high B flat each show distinct harmonic content and amplitude characteristics. Panel (d) overlays all three PSDs for direct comparison across octaves, highlighting differences in harmonic spacing, amplitude decay, and spectral noise.

Figure 4.4 (a,b,c) shows the power spectral densities (PSDs) for the low, middle, and high B flats. The low B flat (a), has the densest harmonic content within the 0–2500 Hz range. The first five harmonics are sharp and distinct, indicating strong harmonic behavior. Beyond this range, the harmonics remain clear, though their amplitudes gradually decrease, particularly above 800 Hz.

The spectrum alternates between regions of stronger and weaker harmonic energy, giving it a subtle bump-like shape similar to the bump structure seen in formants. The consistent spacing and clarity of the peaks indicate that the low B flat remains closely harmonic across its full range.

The middle B flat (b), played with mostly open tone holes, shows its strongest peak at the fundamental, followed by harmonics that exhibit more noticeable noise beginning near 800 Hz. The harmonic peaks are still clearly visible, and a similar bump-like pattern is observed. Although the bumps do not align with those in the low B flat, they reflect a comparable fluctuation in energy.

The high B flat (c), which uses similar fingering to the middle B flat but includes the register key, has the sparsest spectral content of the three. Its peaks are still clearly visible and display consistent harmonic spacing, and noise again becomes prominent around 700–800 Hz. The greatest energy appears at the fundamental, followed by a drop at 1107 Hz and a secondary rise near 1660 Hz, forming another bump-like structure.

Figure 4.4 (d) overlays all three PSDs for direct comparison. This figure highlights the similarities and differences between each octave of the B flat. All three notes show instances of increasing and decreasing energy creating bump-like structures. Also, a significant amount of noise can be seen in each plot starting around 700-800 Hz. This plot helps show the similarities and differences between the spectrum of a B flat played in three different octaves.

4.4.2 Directivity Analysis

The next analysis examined the directivity patterns of the alto saxophone across octaves. The resulting balloon plots are shown in Figure 4.5. Each plot visualizes the directional sound field using both color and shape: red indicates areas of highest sound pressure level, while blue represents the lowest. The contour of the balloon reflects how strongly sound radiates in different directions around the instrument. In this setup, the saxophone was oriented such that the microphone at 270° faced directly into the bell.

The plots are organized into columns by frequency and into rows by register: low B flat (top), middle B flat (middle), and high B flat (bottom). While each column represents the same harmonic relative to its fundamental, the exact frequencies differ slightly (e.g., 2218 Hz, 2225 Hz, 2220 Hz). These differences are a result of small tuning variations that naturally occur between takes, caused by differences in embouchure or air pressure.

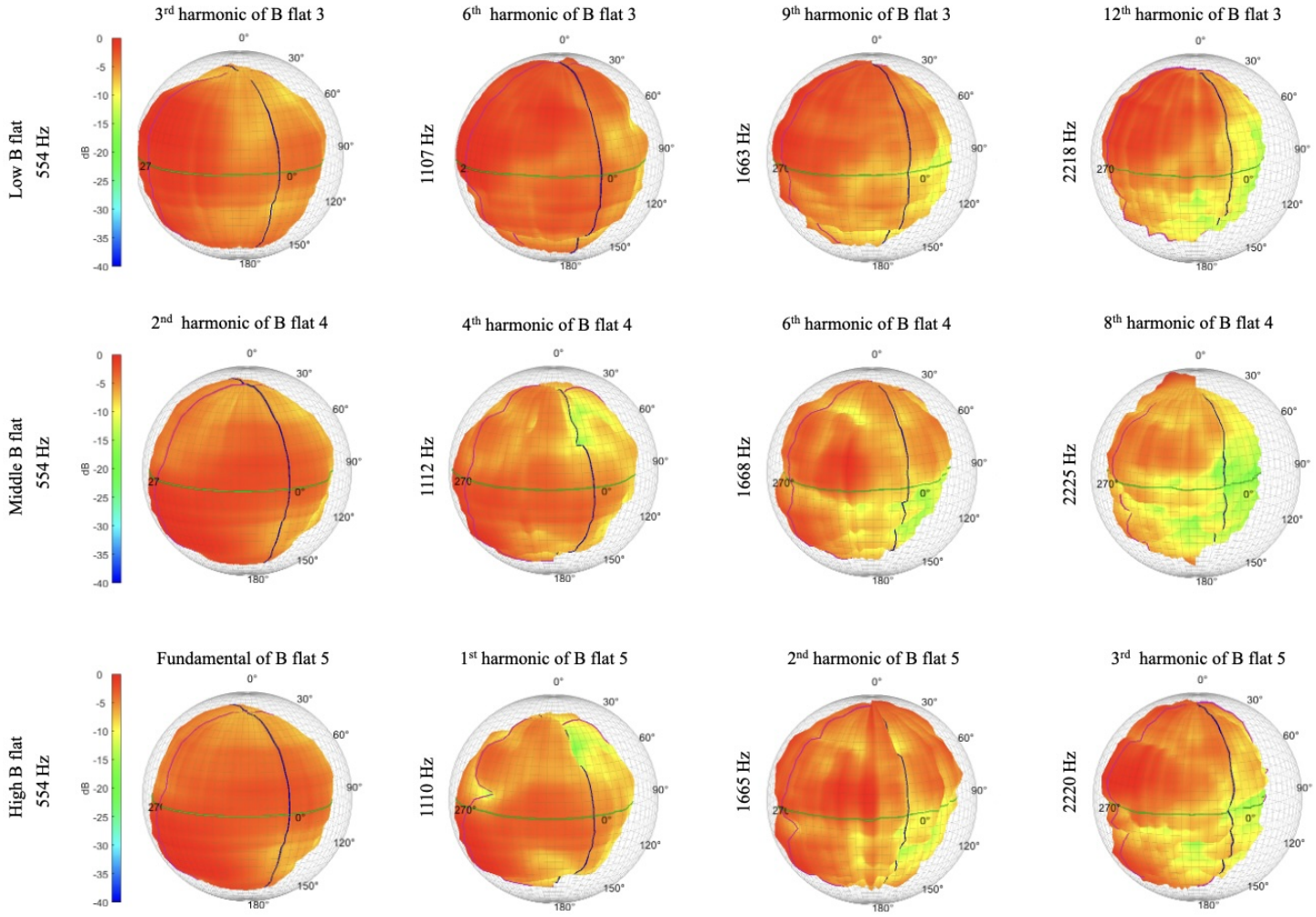

Figure 4.5 The directivity balloon plots from the saxophone while the note B flat was played in three different octaves. The microphones are directly in front of the player at 270°.

The first column shows the results for 554 Hz, the fundamental frequency of the high B flat. At this frequency, there is a large amount of radiation surrounding the instrument, but directly in front of the saxophone, the directivity appears to come from the bottom of the sphere, which roughly corresponds to the location of the bell. While the radiation is most likely not coming directly from the bell, the angled radiation from higher on the instrument leads to increased radiation towards the bottom of the sphere. This trend is consistent with that of the angled radiation from a phased array [60].

When looking at the directivity of the low B flat at 554 Hz, there is strong overall radiation, but the directionality is noticeably different from that of the middle and high B flats. Instead of the sound projecting toward the bottom of the balloon plot, the radiation is concentrated toward the top. This aligns with the physical orientation of the instrument, where the bell is angled upward. It suggests that the bell is the dominant source of radiation at this frequency and directs sound upward into the surrounding space.

As frequency increases, similar trends emerge across the B flats in different octaves. The high and middle B flats generally have similar directivity patterns, with stronger radiation near the bottom of the balloon plot, likely due to their similar fingerings. Across frequency, the low B flat shows the largest radiation towards the top of the plot. An exception to these trends occurs around 2220 Hz. The middle and high B flats show a larger amount of upward radiation, more similar to the patterns expected from the low B flat.

Overall, this analysis shows that register and fingering can have a clear impact on saxophone directivity, even when the B flat is played across octaves. In general, the high and middle B flats share nearly identical directivity patterns, due to their similar fingerings. At lower frequencies, a large portion of radiation is pointed towards the bottom of the bell, but as frequency increases, an increase in radiation is seen coming from the top of the instrument. The low B flat, on the other

hand, shows radiation patterns that suggest the sound source is higher up on the instrument due to the bore geometry of the saxophone.

4.5 Conclusion

This chapter explored how a change in register affects the harmonic structure and directivity of the alto saxophone when playing a B flat in three octaves. Although each note shares a note name, the spectral content and radiated sound field vary across registers. Harmonic analysis revealed that the low B flat produces the densest and most structured spectrum, while higher octave notes display less harmonic content and greater spectral leakage. Directivity balloon plots showed that the location and intensity of sound radiation shift with register, influenced by tone hole configuration and possibly wall vibrations or leakage points on the instrument. The low B flat, despite having all tone holes closed, radiated more from the body than the bell at certain frequencies. These findings suggest that the relationship between pitch, tone hole configuration, and sound radiation is complex. Although this study does not explicitly compute the acoustic center, the results suggest that the effective source location may vary with frequency and register, which is an important consideration for recording, simulation, and performance applications.

Chapter 5

Conclusion and Future Work

5.1 Summary of Research Objectives

The objective of this thesis was to investigate how a few musical instruments radiate sound, with a focus on directivity. The second chapter of this work analyzed the directivity of several percussion instruments, including the bass drum, triangle, and open snare, using different measurement and analysis techniques for each test. To the author's knowledge, high-resolution directivity data had not previously been collected on these instruments. The results help explain how the construction and playing methods influence radiation properties of these instruments.

The third chapter focused on glockenspiel radiation and vibration, while keeping the instrument in its standard mounting configuration. This was done to create a realistic analysis of the bar in a performance setting, rather than the idealized free-free conditions used in prior studies.

Finally, chapter four examined characteristics of the alto saxophone, specifically looking at the harmonic structure and directivity of the instrument when playing a B flat in three octaves. This analysis aimed to understand how the tone holes and frequency content affect the directivity of sound, offering insights into source centering and frequency-dependent acoustic behavior.

5.2 Key Findings by Chapter

Percussion Instruments Directivity (Chapter 2)

The analysis completed in Chapter 2 looked at the directivity of three different percussion instruments: the bass drum, the triangle, and the open snare. All of the instruments showed different radiation characteristics that reflect how they produce sound at different frequencies. These results highlight the importance of considering frequency content, structural design, and striking method when analyzing percussion instruments.

The bass drum showed strong low-frequency dipole-like behavior that transitioned to omnidirectional spreading at mid frequencies and directional spreading at high frequencies. The triangle exhibited highly directional lobing, especially at higher frequencies, due to its rigid, open-frame design. The open snare demonstrated frequency-dependent directivity shaped by interactions between the drumheads, shell, and cavity. These results demonstrate that percussion instruments exhibit diverse and complex radiation behaviors. Their directivity is influenced by a combination of factors, including structural geometry, material properties, and the way they are excited. This chapter contributes valuable high-resolution directivity data for these instruments, which is largely absent in existing literature, and provides a framework for understanding how frequency content, structural design, and striking technique affect acoustic output.

Glockenspiel Radiation and Directivity (Chapter 3)

The glockenspiel analysis presented in Chapter 3 demonstrated that directivity is highly dependent on mounting configuration. At low frequencies, the directivity of the full glockenspiel closely resembled that of a single bar mounted with a rigid baffle, indicating that the baffle constrained the motion similarly to the full instrument frame. However, as frequency increased, the baffled individual bar began to exhibit radiation patterns more closely aligned with the unbaffled configuration, suggesting

that higher-frequency modes are less influenced by boundary constraints and more governed by the bar's inherent vibrational behavior.

Scanning laser Doppler vibrometry was used to investigate the modal properties of an individual bar, providing detailed visualizations of its vibrational modes. The fundamental bending modes agreed well with classical beam theory, reinforcing the expected behavior of free-free bars. The torsional modes also aligned with theoretical predictions, but showed less agreement with previous experimental studies, potentially due to differences in mounting or excitation.

These findings emphasize the importance of considering real-world conditions when interpreting the acoustic behavior of glockenspiel bars. In particular, the mounting configuration plays a role in shaping both vibrational and radiative characteristics.

Alto Saxophone (Chapter 4)

This chapter explored how the alto saxophone radiates sound when playing a B flat across three different octaves. Harmonic spectra remained similar between registers. Each B flat showed clear peaks with consistent spacing.

The directivity analysis showed that, for most frequencies, the middle and high B flats exhibited nearly identical radiation patterns, suggesting a source distribution similar to that of a phased array, where multiple open tone holes act as individual radiators along the instrument's body. In contrast, the low B flat radiated primarily from the bell, with a strong upward projection that appeared at the top of the balloon plots due to the saxophone's bore geometry.

These findings highlight the importance of considering harmonic structure and fingering when analyzing saxophone acoustics and provide valuable insight for applications in source modeling, microphone placement, and spatial audio design.

5.3 Contributions to Musical Acoustics

This research advances the field of musical acoustics by providing high-resolution directivity measurements of percussion and woodwind instruments under realistic playing conditions. For percussion, it offers detailed examinations of how mounting configurations affect sound radiation, highlighting the need to account for structural support and excitation method in acoustic modeling. By analyzing mounted instruments such as the bass drum, triangle, and open snare, this study captures the nuances of how these instruments radiate in performance contexts, providing data that can inform stage design, microphone placement, and virtual acoustic simulations.

The glockenspiel study contributes to musical acoustics by highlighting the importance of mounting conditions in shaping sound radiation. By comparing directivity in both full and isolated bar setups, the results inform more accurate modeling of mallet percussion instruments in real-world configurations. The findings are particularly relevant for designers and recording engineers who must account for how these instruments radiate in ensemble and solo contexts. Additionally, the vibrometry data offer a useful benchmark for refining theoretical models used in acoustical simulations and instrument development.

Research on the alto saxophone offers new understanding of how register affects radiation patterns, showing that tone hole configuration and harmonic content shape the effective source location. The study demonstrates that the low B flat radiates primarily from the bell, while the middle and high B flats behave like distributed sources along the instrument's body, similar to a line array. Spectral analysis also revealed how harmonic structure evolves with register, influencing the directionality of radiated sound. These findings can help guide more effective microphone placement, improve physical modeling of wind instruments, and inform performance and recording techniques that account for register-dependent sound projection.

Together, these contributions, which will be added to an instrument directivity database at Brigham Young University, will help bridge experimental acoustics and practical musical applica-

tions, offering data and insights valuable for performers, acousticians, and instrument designers alike.

Appendix A

Glockenspiel SLDV Scans

A.1 Free-Free Bar Scans

This section presents scanning laser Doppler vibrometry (SLDV) data collected from an individual glockenspiel bar, the D7, suspended in a free-free boundary condition. Each bar was hung using thin fishing wire to reduce interference. To excite the bar, a MACKIE speaker was used to sweep through a range of frequencies, and the resulting motion was captured using a scanning laser system. These measurements were conducted to isolate and visualize the vibrational modes of the bars without the influence of mounting hardware or frame constraints. The free-free configuration allows for comparison with theoretical beam models and helps identify the fundamental bending and torsional modes. The following figures show mode shapes across a range of frequencies, offering insight into how each bar naturally vibrates when unconstrained.

Free-Free Bar: 2,374 Hz

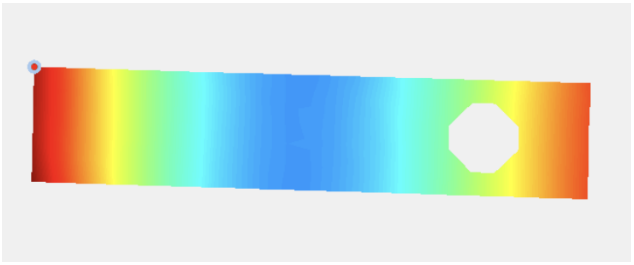

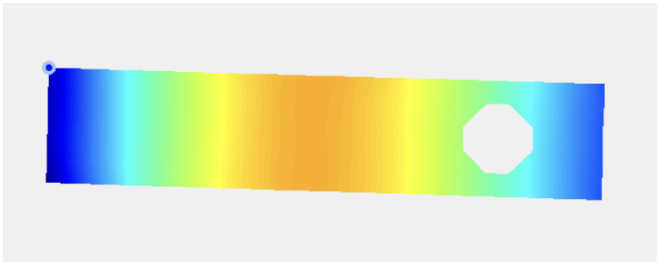

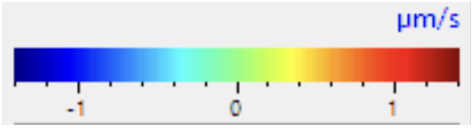

Free-Free Bar: 5,713 Hz

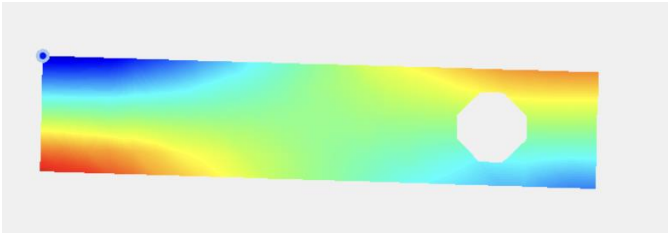

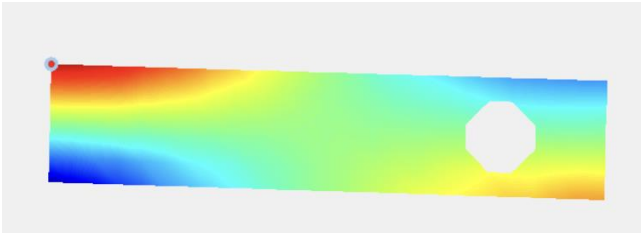

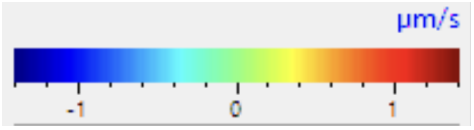

Free-Free Bar: 6,378 Hz

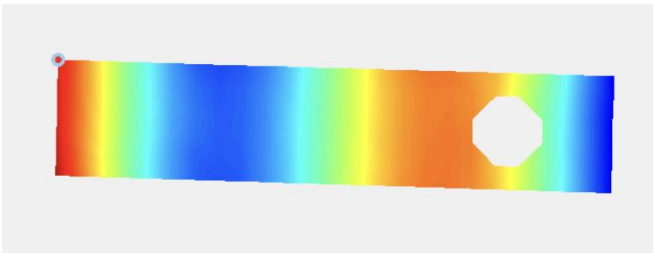

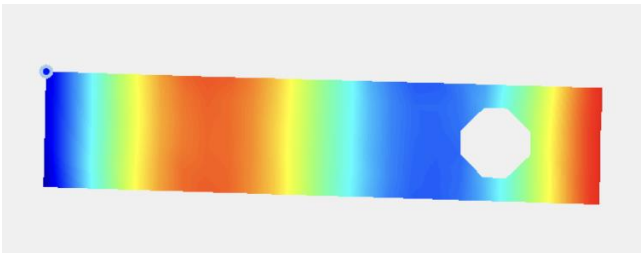

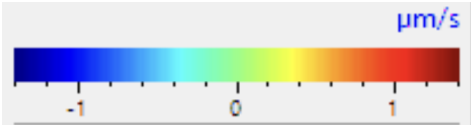

Free-Free Bar: 11,553 Hz

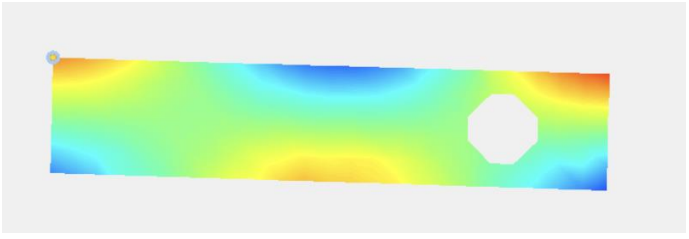

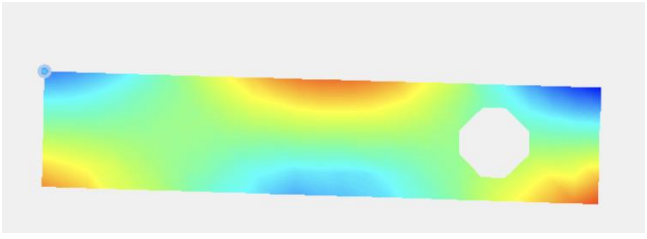

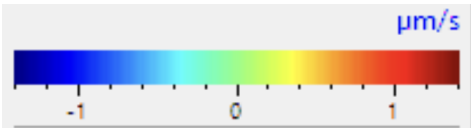

Free-Free Bar: 12,000 Hz

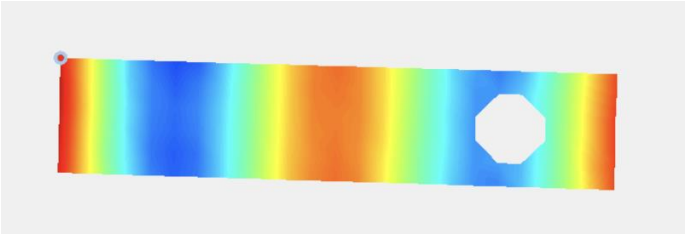

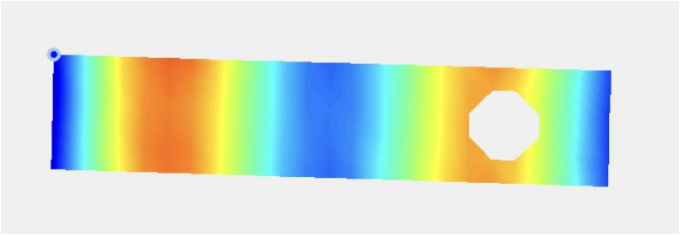

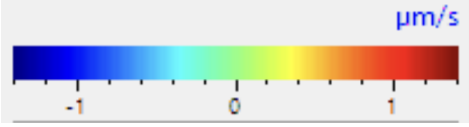

Free-Free Bar: 17,623 Hz

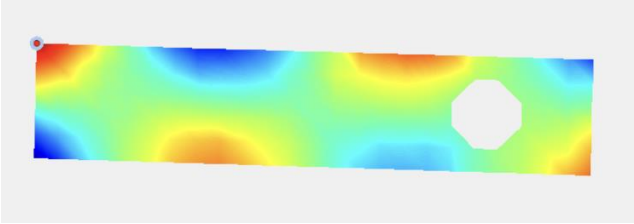

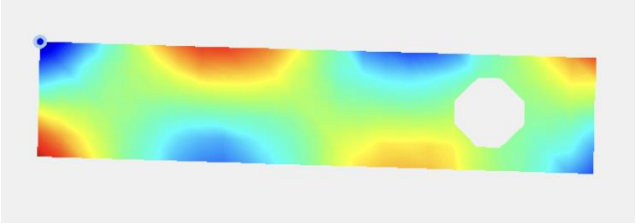

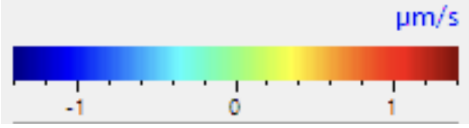

Free-Free Bar: 19,318 Hz

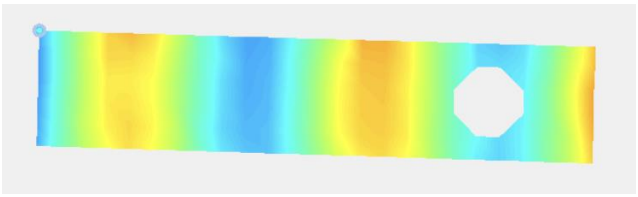

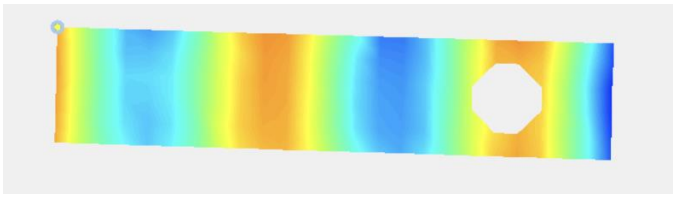

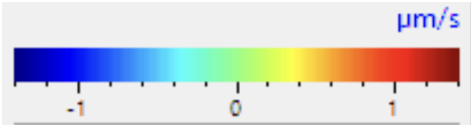

A.2 In-Frame Bar Scans

The second section includes SLDV scans of bars mounted within the full glockenspiel frame. A MACKIE speaker was again used to excite the bar, but it remained in the frame for this set of tests. These measurements were taken to assess how the mounting configuration influences bar vibration and radiation in a realistic performance setup. Unlike the free-free case, the in-frame condition introduces boundary constraints that affect modal behavior, damping, and radiative efficiency. By comparing these results to the free-free scans, the impact of mounting on vibrational mode shapes and frequencies becomes apparent. The figures below document the observed changes across several bars and frequencies

In-Frame Bar: 2373 Hz

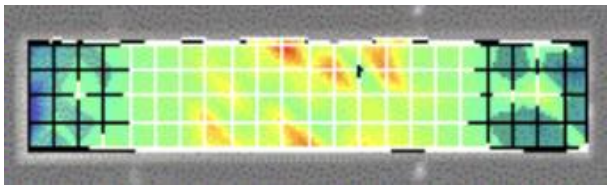

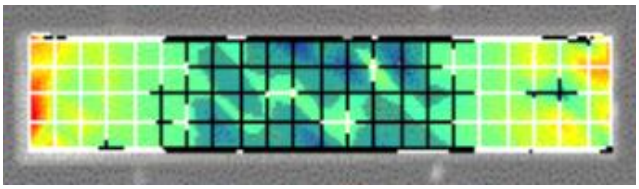

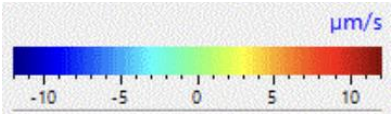

In-Frame Bar: 5742 Hz

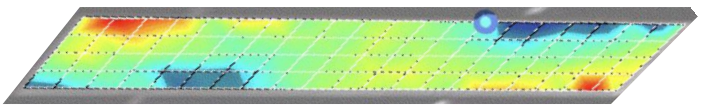

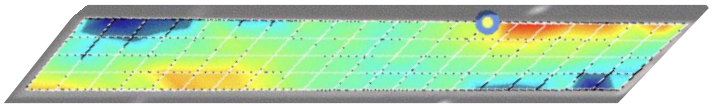

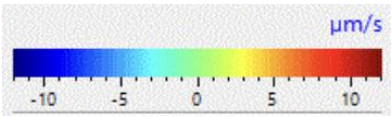

In-Frame Bar: 6388 Hz

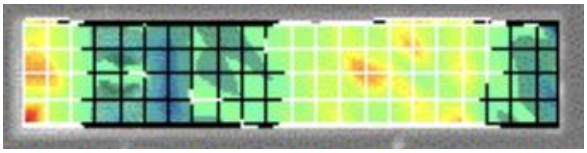

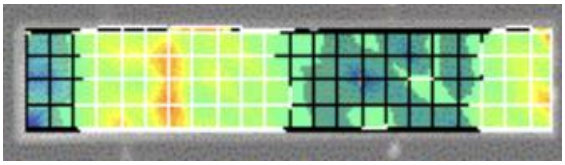

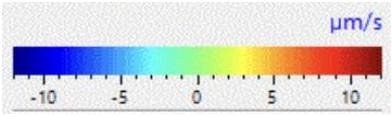

In-Frame Bar: 7077 Hz

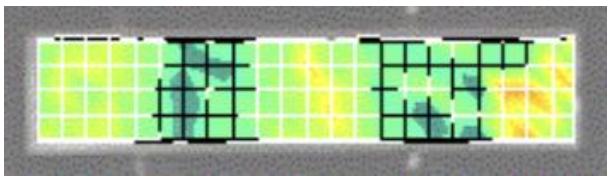

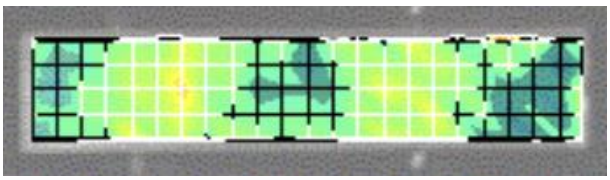

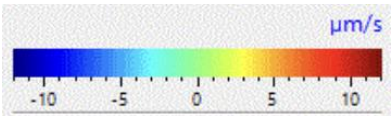

Appendix B

Glockenspiel Power Spectral Density

To better understand the spectral content of the glockenspiel across its full range, individual power spectral density (PSD) plots were generated for each note. These plots reveal the distribution of energy across frequency for every bar, providing insight into harmonic structure, resonant behavior, and how spectral features evolve throughout the instrument. This analysis complements the directivity and vibrometry studies by highlighting the unique frequency content of each pitch, which plays a key role in how the glockenspiel radiates sound and contributes to its characteristic timbre.

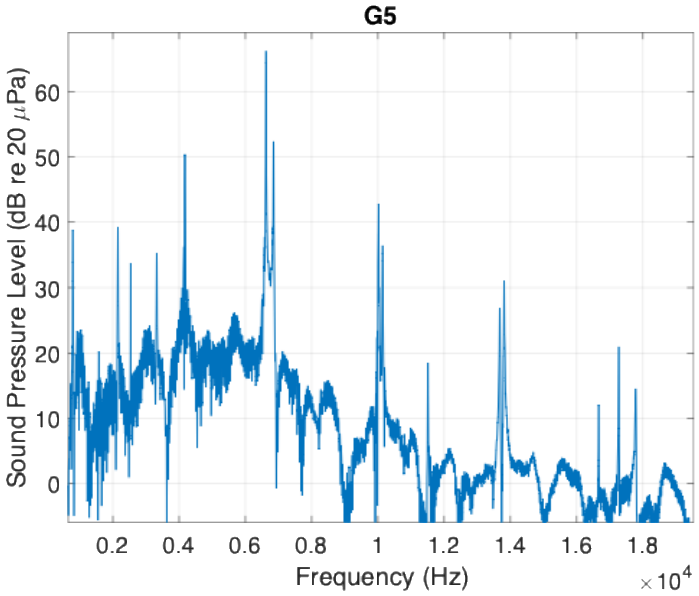
G5
Sound Pressure Level (dB re 20 μPa)
Frequency (Hz)
$\times 10^4$

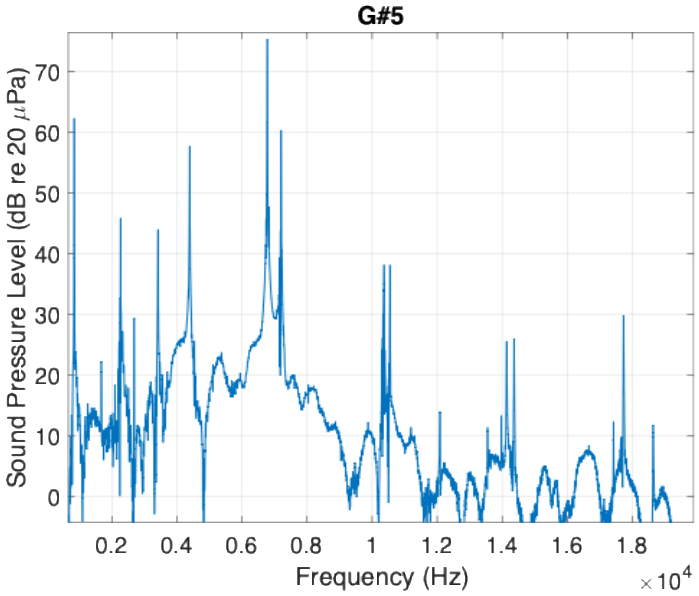
G#5
Sound Pressure Level (dB re 20 μPa)
Frequency (Hz)
$\times 10^4$

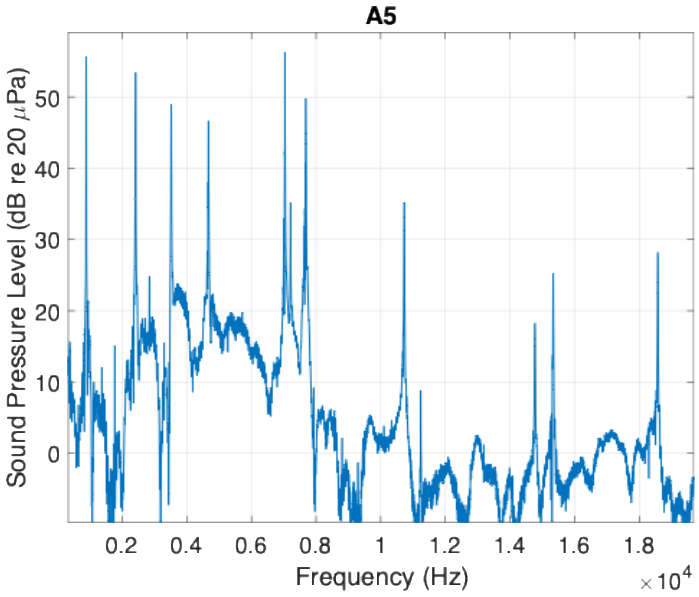
A5
Sound Pressure Level (dB re 20 μPa)
Frequency (Hz)
$\times 10^4$

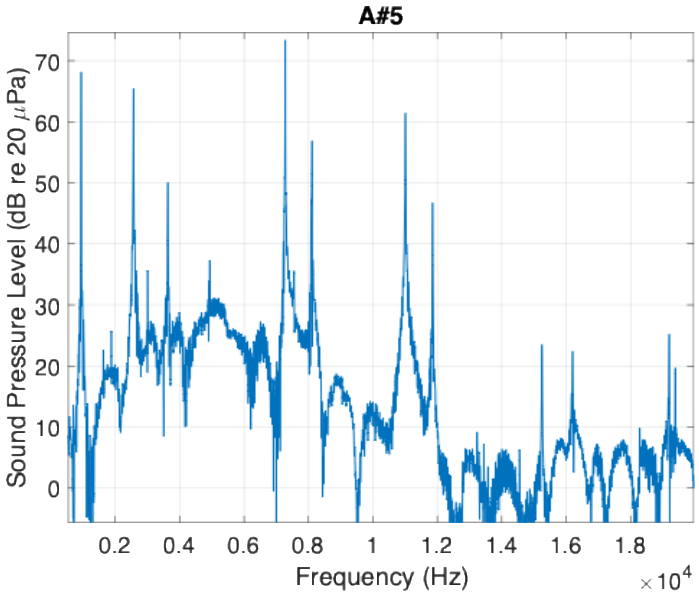
A#5
Sound Pressure Level (dB re 20 μPa)
Frequency (Hz)
$\times 10^4$

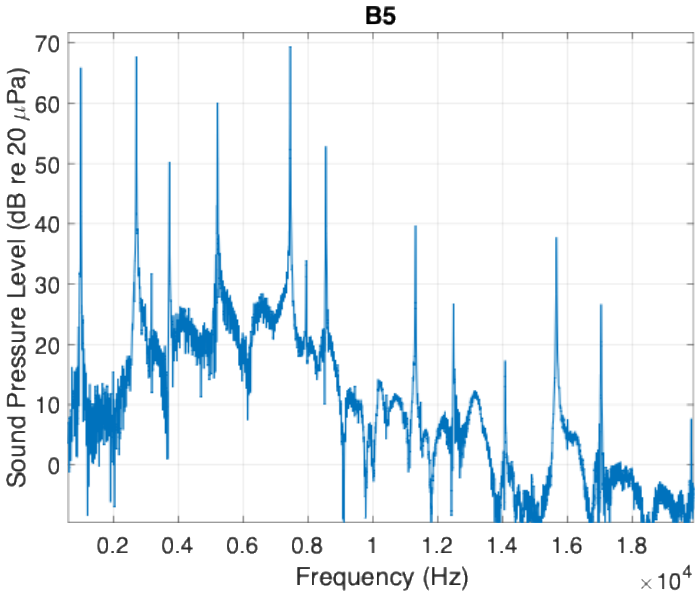
B5
Sound Pressure Level (dB re 20 μPa)
70
60
50
40
30
20
10
0
0.2
0.4
0.6
0.8
1
1.2
1.4
1.6
1.8
Frequency (Hz)
$\times 10^4$

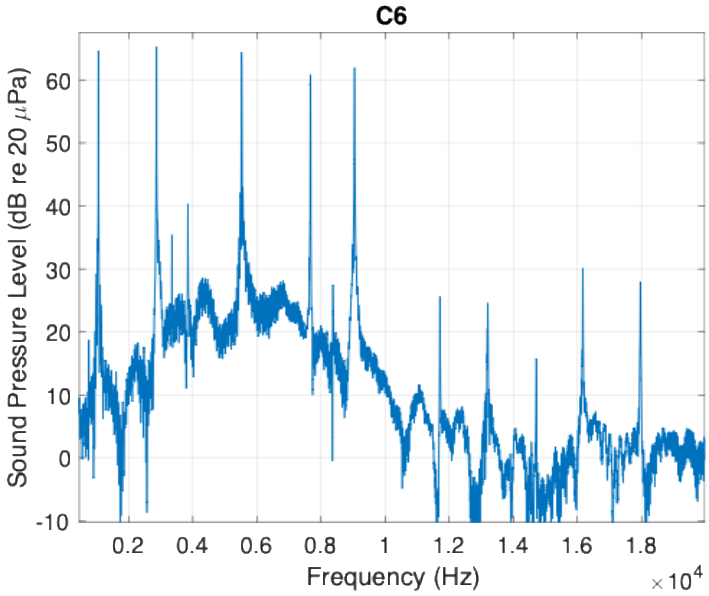
C6
Sound Pressure Level (dB re 20 μPa)
60
50
40
30
20
10
0
-10
0.2
0.4
0.6
0.8
1
1.2
1.4
1.6
1.8
Frequency (Hz)
$\times 10^4$

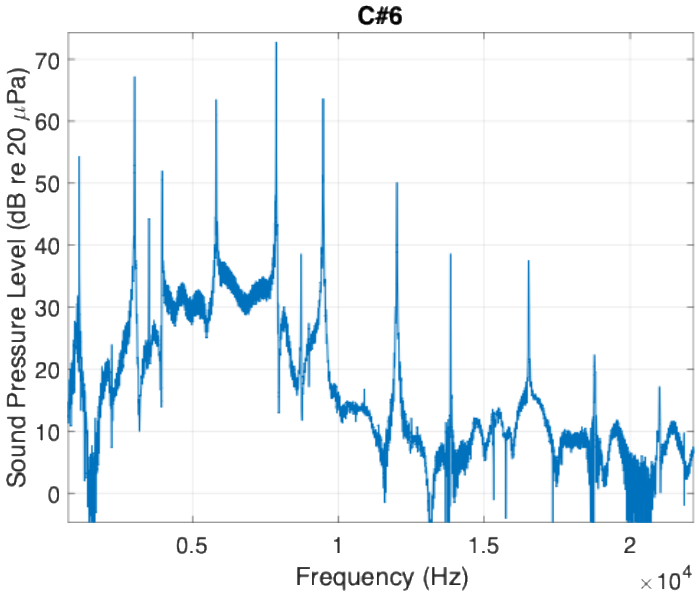
C#6
Sound Pressure Level (dB re 20 μPa)
70
60
50
40
30
20
10
0
0.5
1
1.5
2
Frequency (Hz)
$\times 10^4$

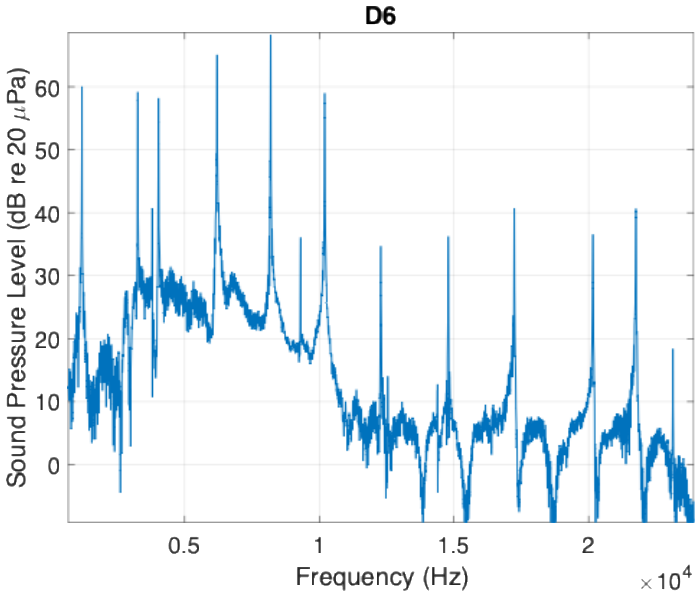
D6
Sound Pressure Level (dB re 20 μPa)
60
50
40
30
20
10
0
0.5
1
1.5
2
Frequency (Hz)
$\times 10^4$

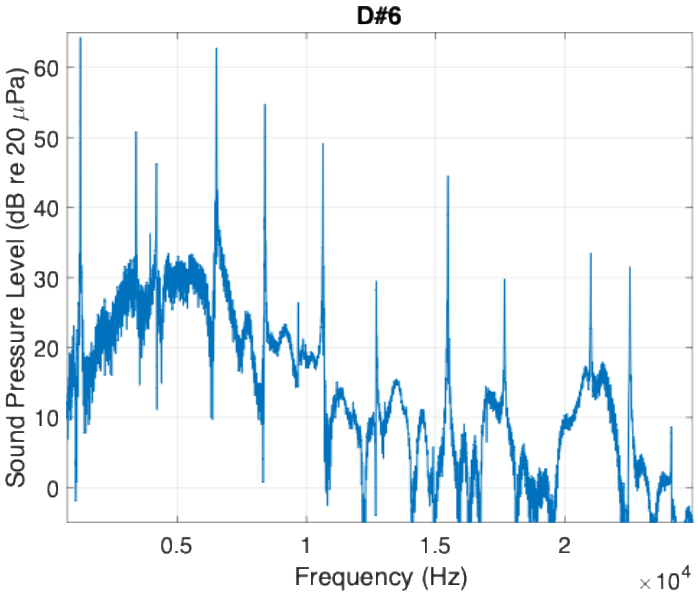
D#6
Sound Pressure Level (dB re 20 μPa)
Frequency (Hz)
$\times 10^4$

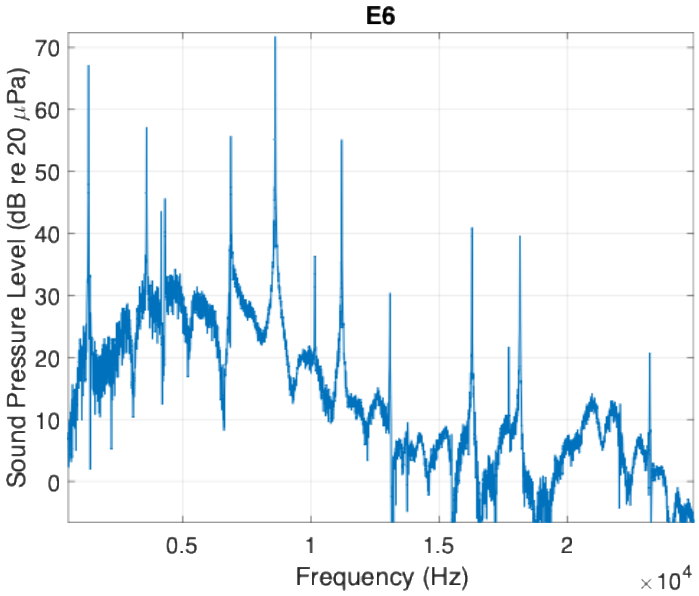
E6
Sound Pressure Level (dB re 20 μPa)
Frequency (Hz)
$\times 10^4$

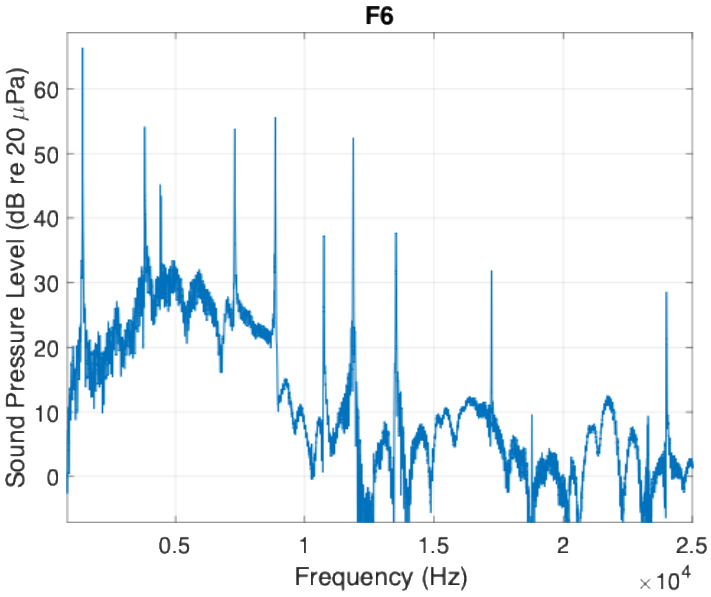
F6
Sound Pressure Level (dB re 20 μPa)
Frequency (Hz)
$\times 10^4$

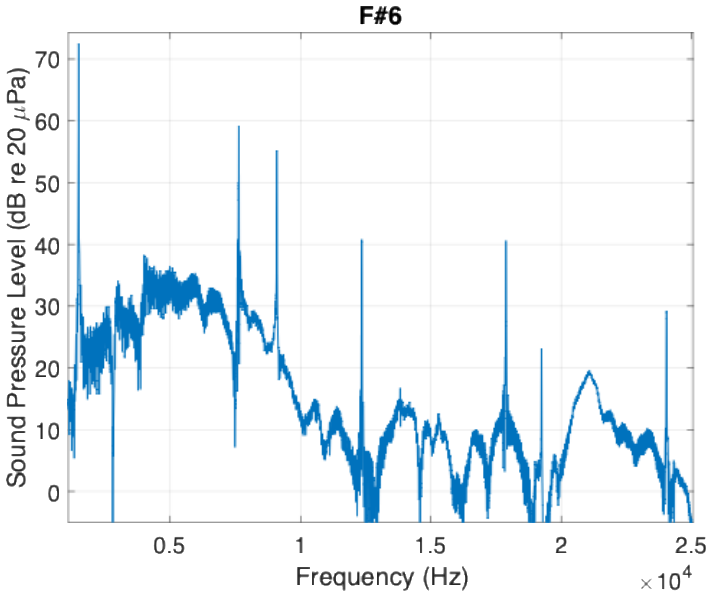
F#6
Sound Pressure Level (dB re 20 μPa)
Frequency (Hz)
$\times 10^4$

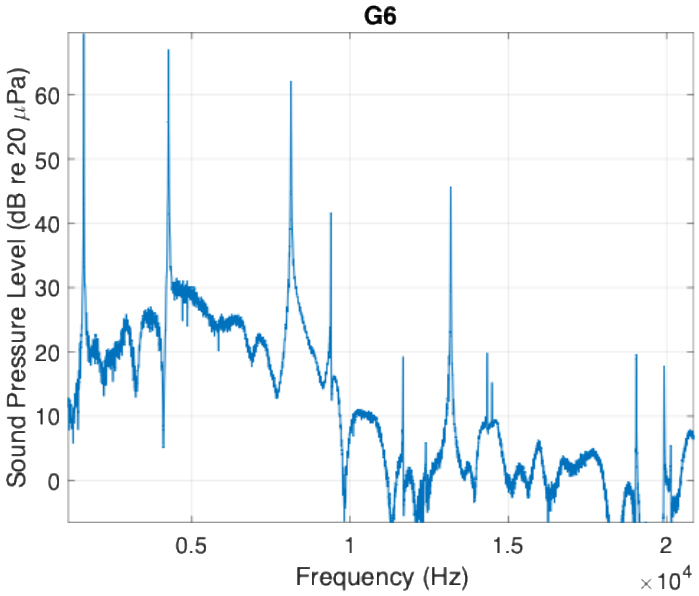
G6
Sound Pressure Level (dB re 20 μPa)
Frequency (Hz)
$\times 10^4$

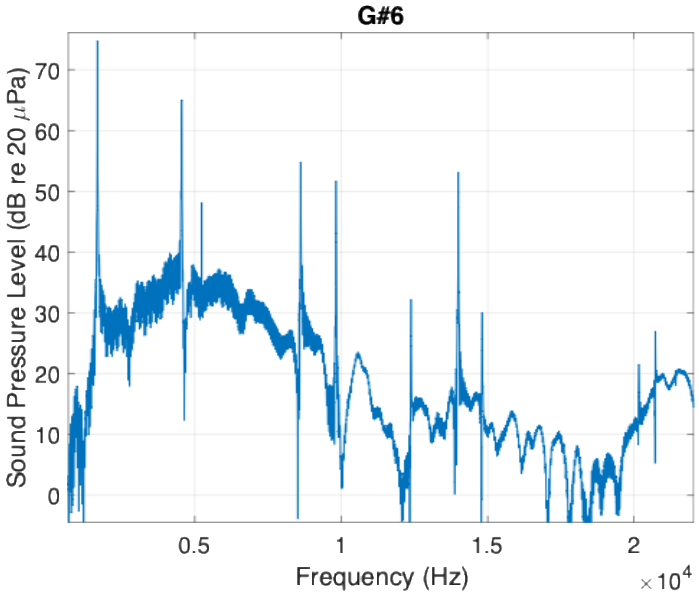
G#6
Sound Pressure Level (dB re 20 μPa)
Frequency (Hz)
$\times 10^4$

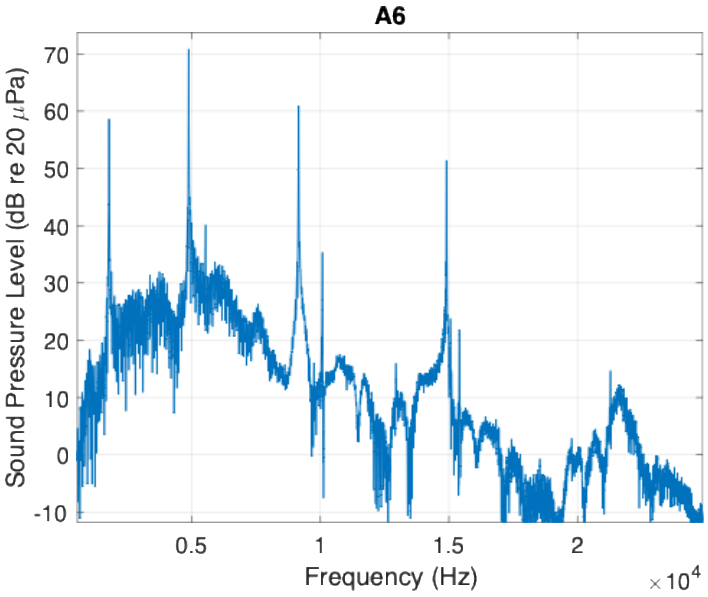
A6
Sound Pressure Level (dB re 20 μPa)
Frequency (Hz)
$\times 10^4$

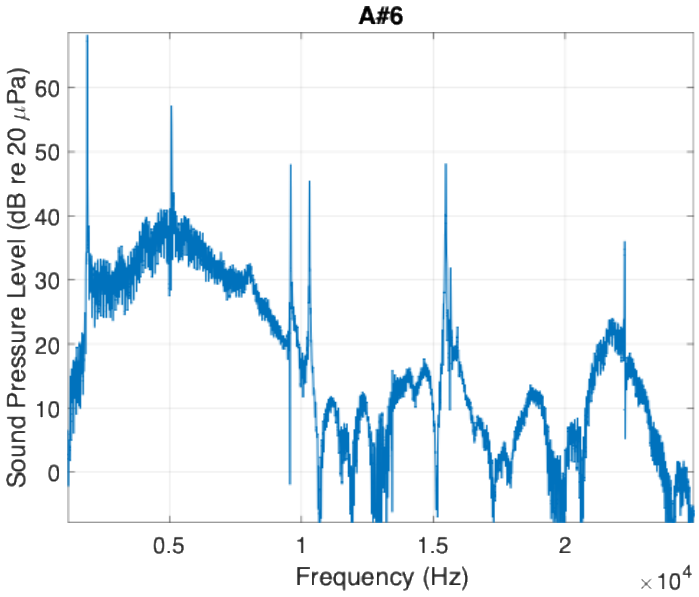
A#6
Sound Pressure Level (dB re 20 μPa)
Frequency (Hz)
$\times 10^4$

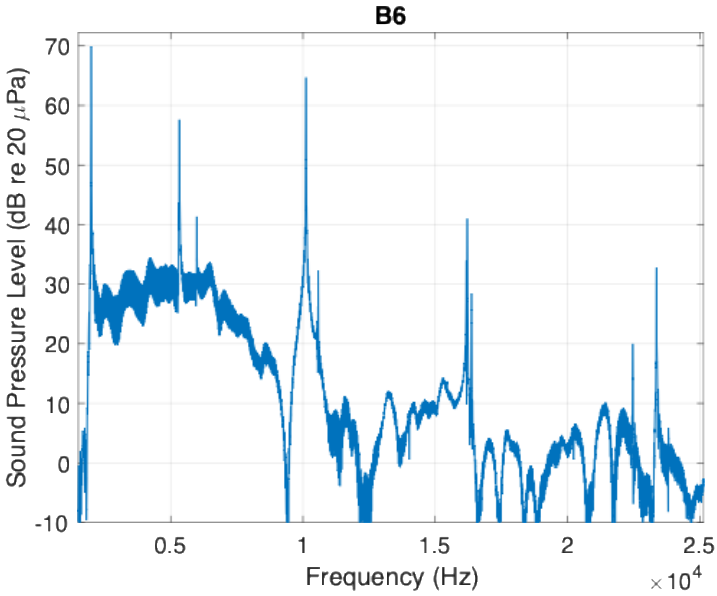
B6
Sound Pressure Level (dB re 20 μPa)
70
60
50
40
30
20
10
0
-10
0.5
1
1.5
2
2.5
Frequency (Hz)
$\times 10^4$

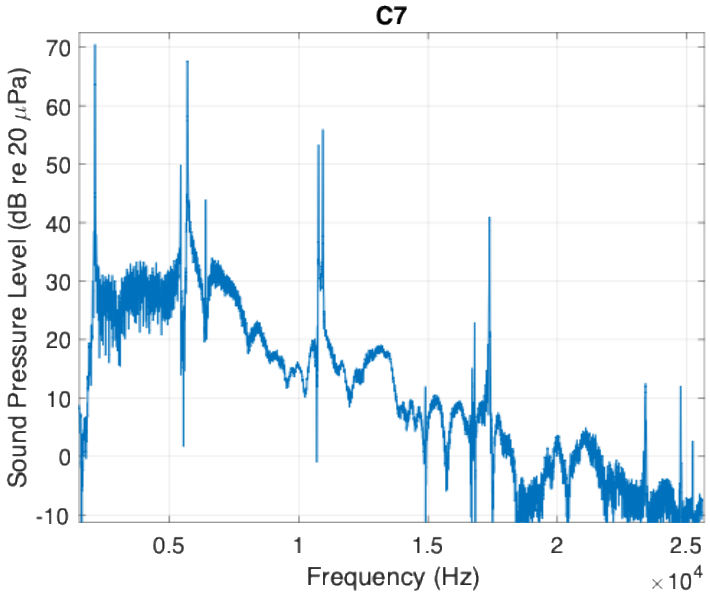
C7
Sound Pressure Level (dB re 20 μPa)
70
60
50
40
30
20
10
0
-10
0.5
1
1.5
2
2.5
Frequency (Hz)
$\times 10^4$

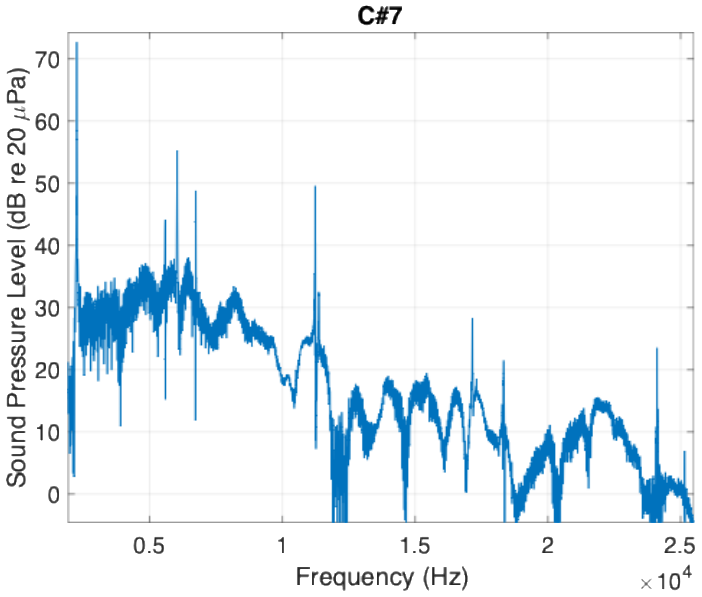
C#7
Sound Pressure Level (dB re 20 μPa)
70
60
50
40
30
20
10
0
0.5
1
1.5
2
2.5
Frequency (Hz)
$\times 10^4$

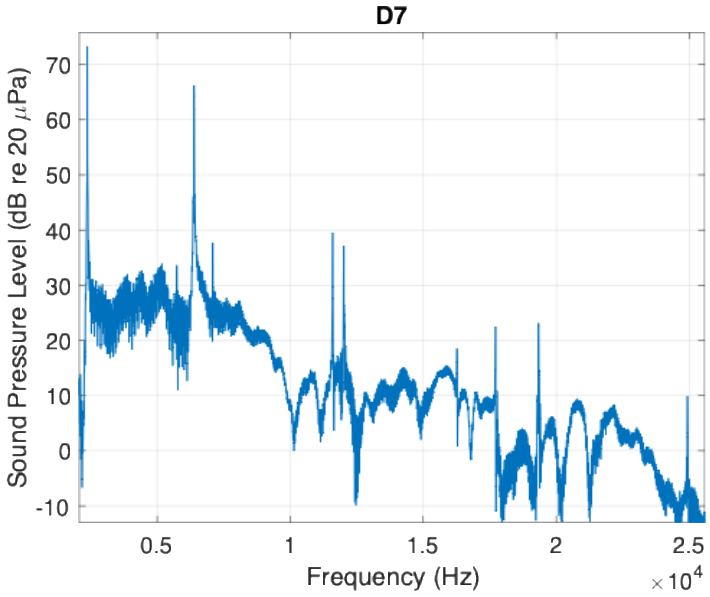
D7
Sound Pressure Level (dB re 20 μPa)
70
60
50
40
30
20
10
0
-10
0.5
1
1.5
2
2.5
Frequency (Hz)
$\times 10^4$

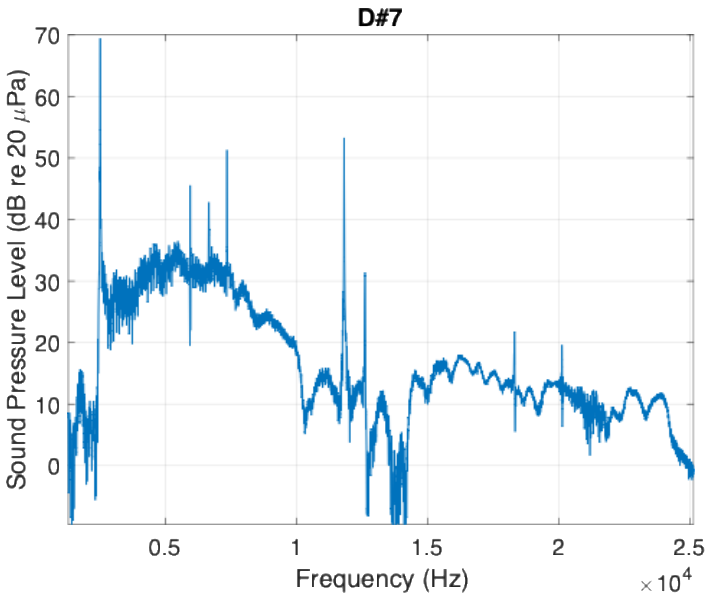
D#7
Sound Pressure Level (dB re 20 μPa)
70
60
50
40
30
20
10
0
0.5
1
1.5
2
2.5
Frequency (Hz)
$\times 10^4$

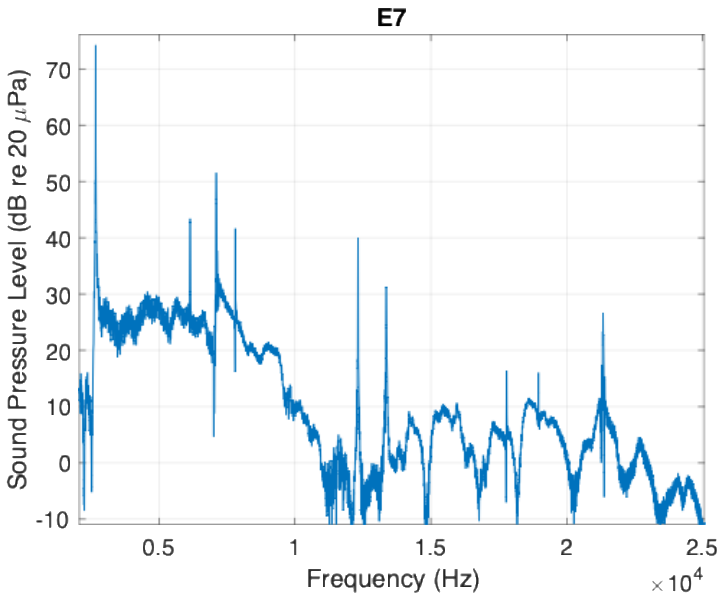
E7
Sound Pressure Level (dB re 20 μPa)
70
60
50
40
30
20
10
0
-10
0.5
1
1.5
2
2.5
Frequency (Hz)
$\times 10^4$

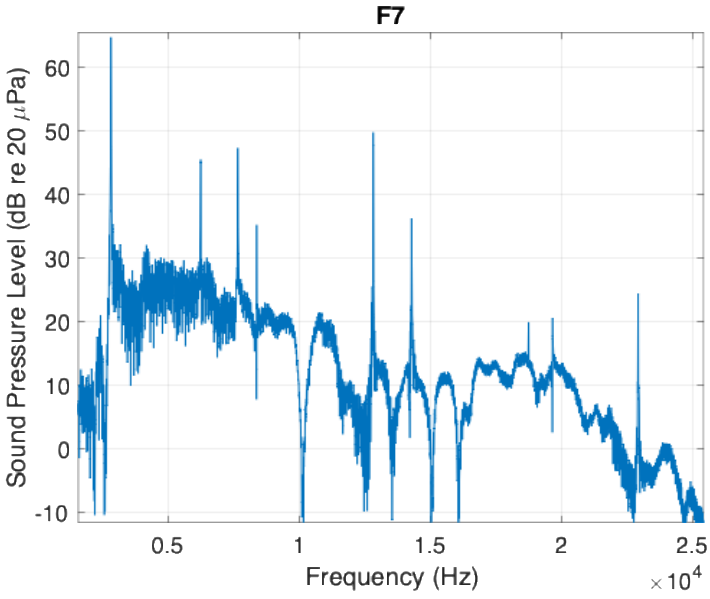
F7
Sound Pressure Level (dB re 20 μPa)
60
50
40
30
20
10
0
-10
0.5
1
1.5
2
2.5
Frequency (Hz)
$\times 10^4$

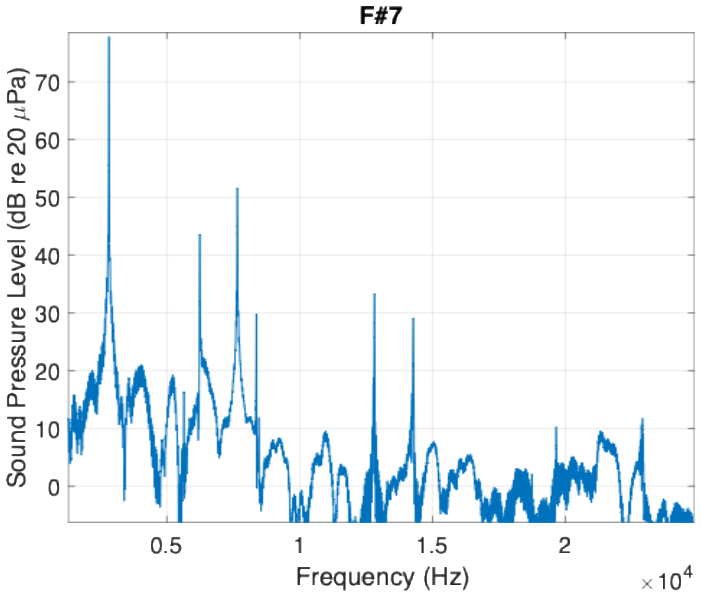
F#7
Sound Pressure Level (dB re 20 μPa)
70
60
50
40
30
20
10
0
0.5
1
1.5
2
Frequency (Hz)
$\times 10^4$

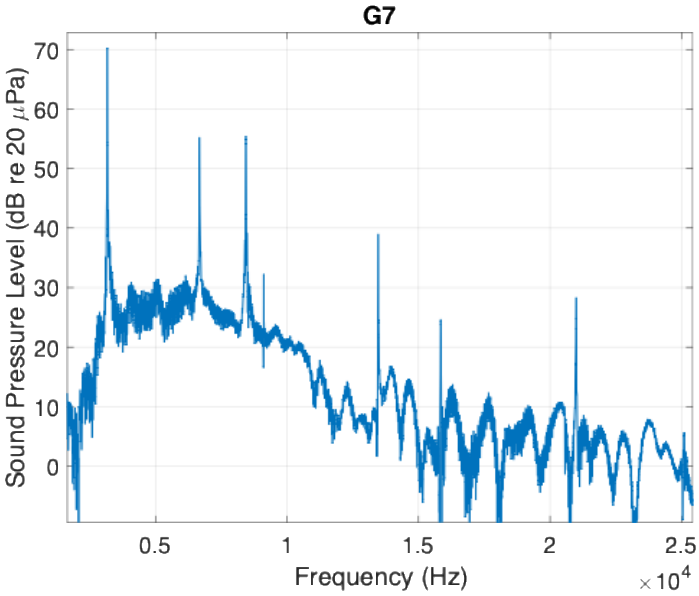
G7
Sound Pressure Level (dB re 20 μPa)
Frequency (Hz)
×10^4

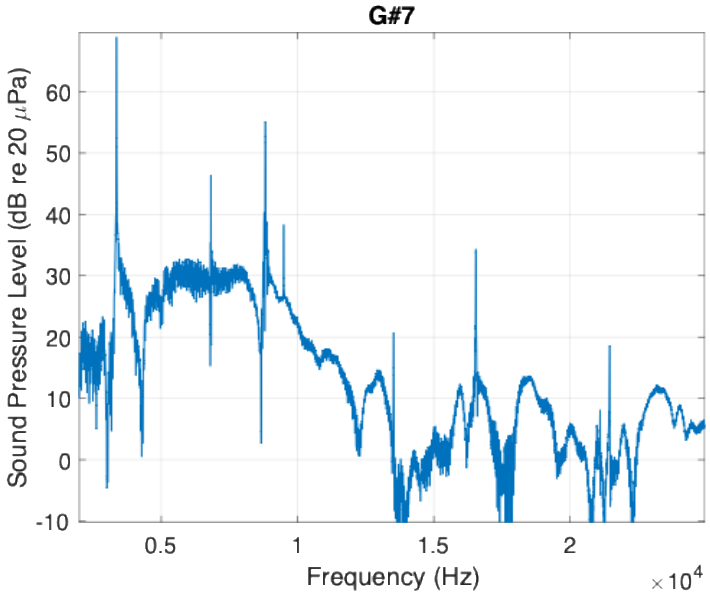
G#7
Sound Pressure Level (dB re 20 μPa)
Frequency (Hz)
×10^4

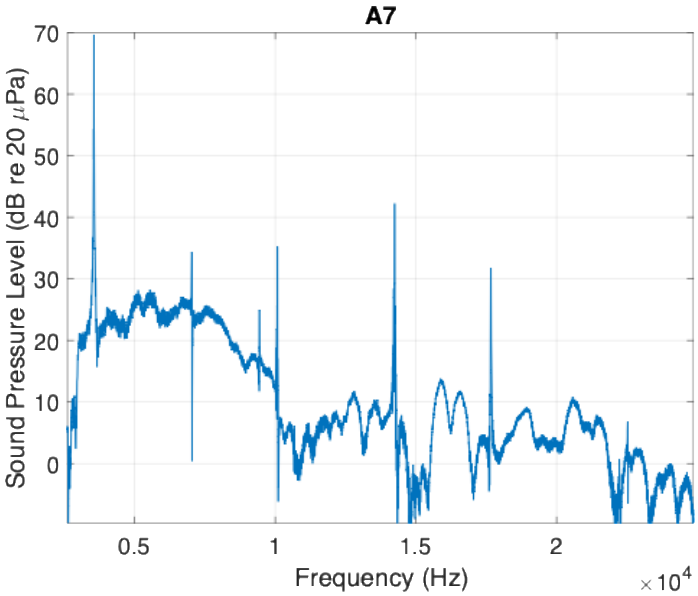
A7
Sound Pressure Level (dB re 20 μPa)
Frequency (Hz)
×10^4

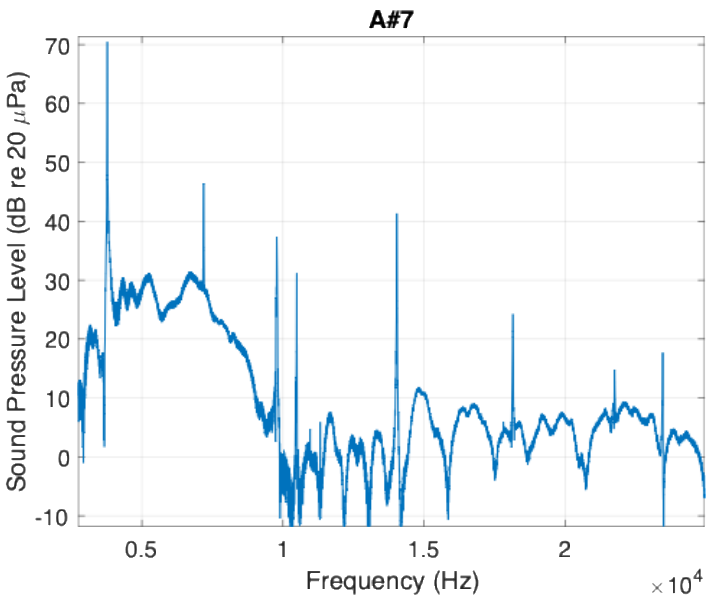
A#7
Sound Pressure Level (dB re 20 μPa)
Frequency (Hz)
×10^4

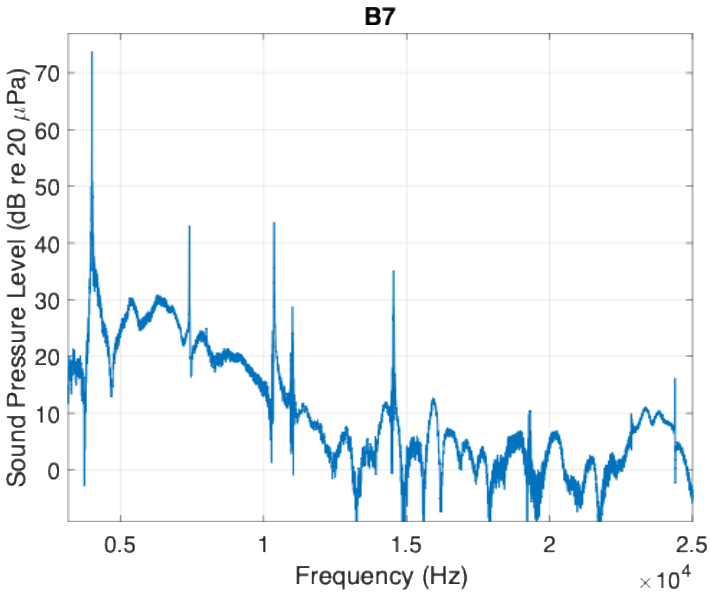
B7
Sound Pressure Level (dB re 20 μPa)
70
60
50
40
30
20
10
0
0.5
1
1.5
2
2.5
Frequency (Hz)
$\times 10^4$

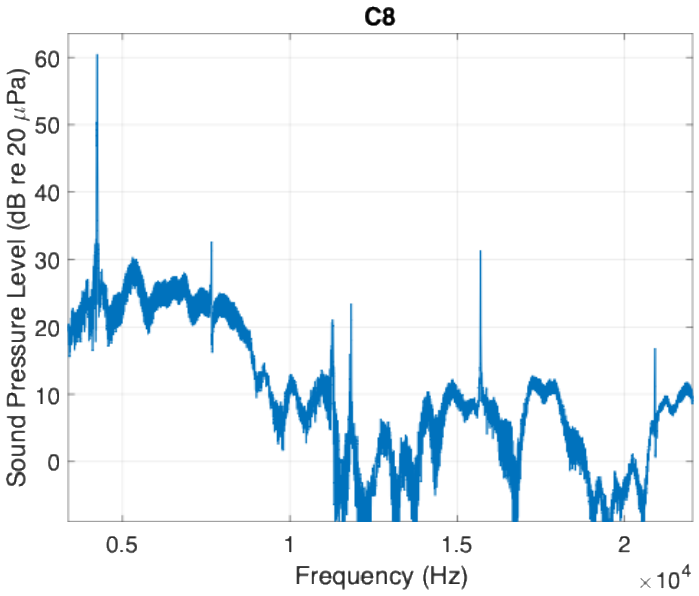
C8
Sound Pressure Level (dB re 20 μPa)
60
50
40
30
20
10
0
0.5
1
1.5
2
Frequency (Hz)
$\times 10^4$

Bibliography

[1] P. R. Cook, “A Database of Measured Musical Instrument Body Radiation Impulse Responses, and Computer Applications for Exploring and Utilizing the Measured Filter Functions,” In *Proceedings of the International Symposium on Musical Acoustics*, (Citeseer, 1998).

[2] F. Otondo and J. H. Rindel, “The Influence of the Directivity of Musical Instruments in a Room,” Acta Acustica united with Acustica **90,** 1178–1184 (2004).

[3] F. Hohl and F. Zotter, “Similarity of musical instrument radiation-patterns in pitch and partial,” In *Proceedings of the 2nd International Symposium on Ambisonics and Spherical Acoustics*, (Paris, France, 2010).

[4] "Remo Fiberskyn Medium FA-1540-00-40 Concert Bass Drum Head," https://www.westmusic.com/remo-fiberskyn-medium-fa-1540-00-40-concert-bass-drum-head-253378, 2024, accessed: 2025-06-02.

[5] Stagg Percussion, "Stagg Triangle – 8" Triangle with beater," https://staggmusic.com/en/products/view/TRI8-8-triangle-with-beater/, accessed: 2025-06-05.

[6] Amro Music Stores Inc., "Saxophone Fingering Chart," https://www.amromusic.com/saxophone-fingering-chart, accessed: 2025-04-30.

[7] Schmitt Music, "Selmer Paris Supreme 92DL Alto Saxophone," https://www.schmittmusic.com/products/selmer-92dl-supreme-alto-saxophone?variant=49078972907813, 2025, accessed: 2025-06-03.

[8] D. A. Russell, J. P. Titlow, and Y.-J. Bemmen, "Acoustic monopoles, dipoles, and quadrupoles: An experiment revisited," American Journal of Physics **67,** 660–664 (1999).

[9] J. G. Tylka, R. Sridhar, and E. Y. Choueiri, "A Database of Loudspeaker Polar Radiation Measurements,", Audio Engineering Society Convention e-Brief 230, Presented at the 139th Convention, 2015, new York, USA.

[10] G. Zhao, K. Shi, and S. Zhong, "Research on Array Structures of Acoustic Directional Transducer," Mathematical Problems in Engineering **2021,** 6670277:1–5 (2021).

[11] T. Knüttel, I. B. Witew, and M. Vorländer, "Influence of "omnidirectional" loudspeaker directivity on measured room impulse responses," The Journal of the Acoustical Society of America **134,** 3654–3662 (2013).

[12] R. C. Edelman, B. E. Anderson, S. D. Bellows, and T. W. Leishman, "Measured high-resolution directivities of guitar amplifiers," The Journal of the Acoustical Society of America **151,** A157–A157 (2022).

[13] M. Denison, capstone project, Brigham Young University, Advisor: Timothy Leishman (unpublished).

[14] G. Weinreich, "Directional tone color," The Journal of the Acoustical Society of America **101,** 2338–2346 (1997).

[15] M. Pezzoli, A. Canclini, F. Antonacci, and A. Sarti, "A Comparative Analysis of the Directional Sound Radiation of Historical Violins," The Journal of the Acoustical Society of America **152,** 354–367 (2022).

[16] T. D. Rossing, J. Yoo, and A. Morrison, "Acoustics of Percussion Instruments: An Update," Acoustical Science and Technology **25,** 414–418 (2004).

[17] N. H. Fletcher and T. D. Rossing, in *The Physics of Musical Instruments*, 2nd ed. (Springer, New York, 2008), Chap. 19.

[18] J. Meyer and translated by U. Hansen, in *Acoustics and the Performance of Music: Manual for Acousticians, Audio Engineers, Musicians, Architects and Musical Instrument Makers*, *Modern Acoustics and Signal Processing* (Springer New York, 2009), Chap. 4.

[19] J. E. Avila, S. D. Bellows, T. W. Leishman, and K. L. Gee, "Directivity analysis of the muted trumpet," Proceedings of Meetings on Acoustics **50,** 035005 (2023).

[20] M. Pollow, G. Behler, and B. Masiero, "Measuring directivities of natural sound sources with a spherical microphone array," In *Proceedings of the NAG/DAGA International Conference on Acoustics*, p. 6S (Rotterdam, Netherlands, 2009).

[21] K. J. Bodon, Master's thesis, Brigham Young University, 2016, all Theses and Dissertations. Paper 5653.

[22] S. D. Bellows, Phd dissertation, Brigham Young University, 2023, all Theses and Dissertations. 10021.

[23] D. Ackermann, F. Brinkmann, and S. Weinzierl, "A Database with Directivities of Musical Instruments," Journal of the Audio Engineering Society **72,** 170–179 (2024).

[24] F. Jacobsen, S. Barrera Figueroa, and K. Rasmussen, "A note on the concept of acoustic center," The Journal of the Acoustical Society of America **115,** 1468–1473 (2004).

[25] S. D. Bellows and T. W. Leishman, "On the low-frequency acoustic center," The Journal of the Acoustical Society of America **153,** 3404– (2023).

[26] S. B. Figueroa, K. Rasmussen, and F. Jacobsen, “The acoustic center of laboratory standard microphones,” The Journal of the Acoustical Society of America **120,** 59–62 (2006).

[27] J.-H. Chang, J. Jensen, and F. Agerkvist, “Shift of the Acoustic Center of a Closed-Box Loudspeaker in a Linear Array: Investigation Using the Beamforming Technique,” Journal of the Audio Engineering Society **63,** 257–266 (2015).

[28] N. R. Shabtai and M. Vorländer, “Acoustic centering of sources with high-order radiation patterns,” The Journal of the Acoustical Society of America **137,** 1947–1961 (2015).

[29] C. Sachs, in *The History of Musical Instruments* (W. W. Norton & Company, New York, 1940), Chap. 1, pp. 25–59, chapter titled "Early Instruments".

[30] D. Ackermann, F. Brinkmann, and S. Weinzierl, “A Database with Directivities of Musical Instruments,” Journal of the Audio Engineering Society **72,** 170–179 (2024).

[31] S. D. Bellows, D. T. Harwood, K. L. Gee, and M. R. Shepherd, “Directional characteristics of two gamelan gongs,” The Journal of the Acoustical Society of America **154,** 1921–1931 (2023).

[32] S. D. Bellows, D. T. Harwood, K. L. Gee, and T. W. Leishman, “Low-frequency directional characteristics of a gamelan gong,” Proceedings of Meetings on Acoustics **50,** 035003 (2023).

[33] J. Pätynen and T. Lokki, “Directivities of Symphony Orchestra Instruments,” Acta Acustica united with Acustica **96,** 138–167 (2010).

[34] H. Fletcher and I. G. Bassett, “Some experiments with the bass drum,” The Journal of the Acoustical Society of America **64,** 499–506 (1978).

[35] T. W. Leishman, S. D. Bellows, C. M. Pincock, and J. K. Whiting, "High-resolution spherical directivity of live speech from a multiple-capture transfer function method," The Journal of the Acoustical Society of America **149,** 1507–1523 (2021).

[36] S. D. Bellows, J. E. Avila, and T. W. Leishman, "Deriving played trumpet directivity patterns from a multiple-capture transfer-function technique," Acta Acustica **9,** 1–17 (2025).

[37] J. Sampson, H. Pavill, and M. Shepherd, "The development of an automated striking device for repeatable percussion strikes," The Journal of the Acoustical Society of America **155,** A254–A255 (2024).

[38] R. Tanigawa, K. Ishikawa, N. Harada, and Y. Oikawa, "How the shape of the musical triangle influences its sound," JASA Express Letters **5,** 053201 (2025).

[39] M. D. Stanciu, S. M. Nastac, V. Bucur, M. Trandafir, G. Dron, and A. M. Nauncef, "Dynamic Analysis of the Musical Triangles—Experimental and Numerical Approaches," Applied Sciences **12,** 6275 (2022).

[40] M. D. Stanciu, S. M. Nastac, V. Bucur, M. Trandafir, G. Dron, and A. M. Nauncef, "Numerical Modal Analysis of Kinked Bars–Triangle Case of Study," In *IOP Conference Series: Materials Science and Engineering*, **1182,** 012074 (IOP Publishing, 2021).

[41] S. Bilbao, "Time domain simulation and sound synthesis for the snare drum," The Journal of the Acoustical Society of America **131,** 914–925 (2012).

[42] N. Poddar, "Resonant Reverberations: Material Influence on Sound Quality in Percussion Instrument Design and Performance," International Journal of Advanced Research **12,** 251–264 (2024).

[43] T. D. Rossing, I. Bork, H. Zhao, and D. O. Fystrom, "Acoustics of snare drums," The Journal of the Acoustical Society of America **92,** 84–94 (1992).

[44] Vienna Symphonic Library, "Glockenspiel - Vienna Symphonic Library Academy," https://www.vsl.co.at/academy/percussion/glockenspiel, accessed: March 6, 2025.

[45] R. Vetter, "Musical Instruments Collection: Item 1825," https://omeka-s.grinnell.edu/s/MusicalInstruments/item/1825, accessed: 2025-03-10.

[46] Yamaha Music, "Choose the Right Mallet," https://hub.yamaha.com/music-educators/instruments/perc/choose-the-right-mallet/, 2023, accessed: 2025-04-04.

[47] M. E. Jones, K. L. Gee, and J. Grimshaw, "Vibrational characteristics of Balinese gamelan metallophones," The Journal of the Acoustical Society of America **127,** EL197–EL202 (2010).

[48] W. Blake, "The radiation from free-free beams in air and in water," Journal of Sound and Vibration **33,** 427–450 (1974).

[49] A. Akay, M. Bengisu, and M. Latcha, "Transient acoustic radiation from impacted beam-like structures," Journal of Sound and Vibration **91,** 135–145 (1983).

[50] L. E. Kinsler, A. R. Frey, A. B. Coppens, and J. V. Sanders, *Fundamentals of Acoustics*, 4th ed. (John Wiley & Sons, New York, 2000), Chap. 3.

[51] S. A. Hambric, "Structural Acoustics Tutorial—Part 1: Vibrations in Structures," Acoustics Today **12,** 12–20 (2016), accessed June 2025.

[52] S. L. Garrett, in *Understanding Acoustics: An Experimentalist's View of Sound and Vibration* (Springer, 2020), Chap. 5, open Access.

[53] D. A. Russell, "Torsional Waves in a Bar," https://www.acs.psu.edu/drussell/Demos/Torsional/torsional.html, 2023, accessed: 2025-03-06.

[54] S. D. Bellows and T. W. Leishman, “Acoustic source centering of musical instrument directivities using acoustical holography,” Proceedings of Meetings on Acoustics **42,** 055002 (2021).

[55] J.-M. Chen, J. Smith, and J. Wolfe, "Acoustics of the Saxophone," https://www.phys.unsw.edu.au/jw/saxacoustics.html, 2023, accessed: 2025-05-17.

[56] D. E. Lucchetta, L. Schiaroli, G. Battista, M. Martarelli, and P. Castellini, “Experimental acoustic modal analysis of a tenor saxophone,” The Journal of the Acoustical Society of America **152,** 2629–2640 (2022).

[57] A. H. Benade and S. J. Lutgen, “The saxophone spectrum,” The Journal of the Acoustical Society of America **83,** 1900–1907 (1988).

[58] E. Ukshini and J. Dirckx, “Acoustic Pressure Distribution and Mode-Specific Analysis Along the Bore of the Alto Saxophone,” Acoustics 7 (2025).

[59] E. A. Petersen, T. Colinot, J. Kergomard, and P. Guillemain, “On the tonehole lattice cutoff frequency of conical resonators: Applications to the saxophone,” The Journal of the Acoustical Society of America **149,** 1752–1763 (2021).

[60] L. E. Kinsler, A. R. Frey, A. B. Coppens, and J. V. Sanders, in *Fundamentals of Acoustics*, 4th ed. (John Wiley & Sons, New York, 2000), Chap. 7.